A shallow rift basin segmented in space and time: The southern San Luis Basin, Rio Grande rift, northern New Mexico, U.S.A.

Benjamin J. Drenth[1]*, V.J.S. Grauch[1], Kenzie J. Turner[2], Brian D. Rodriguez[1], Ren A. Thompson[2], and Paul W. Bauer[3]

[1]U.S. Geological Survey, P.O. Box 25046, MS 964, Denver Federal Center, Denver, CO 80225, U.S.A.

[2]U.S. Geological Survey, P.O. Box 25046, MS 980, Denver Federal Center, Denver, CO 80225, U.S.A.

[3]New Mexico Bureau of Geology and Mineral Resources, New Mexico Institute of Mining and Technology, 801 Leroy Place, Socorro, NM 87801-4796, U.S.A.

**Correspondence should be addressed to: bdrenth@usgs.gov*

ABSTRACT

Interpretation of gravity, magnetotelluric, and aeromagnetic data in conjunction with geologic constraints reveals details of basin geometry, thickness, and spatiotemporal evolution of the southern San Luis Basin, one of the major basins of the northern Rio Grande rift. Spatial variations of low-density basin-fill thickness are estimated primarily using a 3D gravity inversion method that improves on previous modeling efforts by separating the effects of the low-density basin fill from the effects of pre-rift rocks. The basin is found to be significantly narrower—and more complex in the subsurface—than indicated or implied by previous modeling efforts. The basin is also estimated to be significantly shallower than previously estimated. Five distinct subbasins are recognized within the broader southern San Luis Basin. The oldest and shallowest subbasin is the Las Mesitas graben along the northwestern basin margin, formed during the Oligocene transition from Southern Rocky Mountain volcanic field magmatism to rifting. In this subbasin, sediments are estimated to reach a maximum thickness of ~400 m within a north–south elongated structural depression. Other subbasins that likely initially developed during the Miocene are the dominant tectonic features in the southern San Luis Basin. This includes the Tres Orejas subbasin, which formed in the southwestern portion of the basin by the Embudo fault zone and a hypothesized fault zone along its western margin. This subbasin reaches a maximum thickness of ~2 km, as indicated by magnetotelluric and gravity modeling. The Sunshine Valley, Questa, and Taos subbasins occupy the eastern part of the southern San Luis Basin. The southern Sangre de Cristo fault zone is the dominant tectonic feature that controlled their development after ~20 Ma. The east-down Gorge fault zone controlled the western margins of significant parts of these eastern subbasins, although much of the Taos subbasin may be superimposed on the Tres Orejas subbasin. Maximum low-density basin-fill thicknesses are estimated to be 1.2 km for the Sunshine Valley subbasin, 800 m for the Questa subbasin, and 1.8 km for the Taos subbasin. Subbasin-forming tectonic activity along the Gorge fault zone and within the Tres Orejas subbasin ceased by the end of the development of the largely Pliocene Taos Plateau volcanic field. After that, rift-related subsidence became more narrowly centered on the eastern margin of the basin, controlled mainly by the linked Embudo and southern Sangre de Cristo fault zones.

KEY WORDS: aeromagnetic data, gravity modeling, magnetotelluric data, rift basin, Rio Grande rift.

INTRODUCTION

The San Luis Basin extends for roughly 250 km north–south through northern New Mexico and south-central Colorado and is one of the northernmost major basins of the Rio Grande rift (Fig. 1). The present-day geomorphic basin is bounded on the west by the Tusas Mountains in New Mexico and the San Juan Mountains (in Colorado), and on the east by the Sangre de Cristo Mountains (Figs. 1 and 2). The southern boundary is formed by the Picuris Mountains and Cerro Azul. The southern San Luis Basin is here defined as the part of the basin within New Mexico, encompassing the Taos Plateau, Sunshine Valley, and town of Taos, and reaching the eastern margin of the Tusas Mountains.

Despite the critical importance of rift basins for groundwater supplies in this semiarid region (Robson and Banta, 1995; Topper et al., 2003), the general subsurface geometry of the southern San Luis Basin is poorly understood. Studies of geometry and evolution of the southern San Luis Basin are hampered by a paucity of deep drill holes and seismic data over large areas, as well as the burial of important geologic contacts and faults by younger volcanic flows, sedimentary rocks, and sediments. The evolution of rifting in the region has also not

Received 18 April 2019 • Revised submitted 17 July 2019 • Accepted 29 July 2019 • Published online December 2019

Gold Open Access: This paper is published under the terms of the CC-BY license.

Downloaded from https://pubs.geoscienceworld.org/uwyo/rmg/article-pdf/54/2/97/4907139/05402097.pdf
by USGS Library, Benjamin Drenth

been fully described at a regional scale, particularly in terms of the evolution of the rift basin itself. Furthermore, the temporal evolution of the structures bounding the basin and its subbasins has not been fully described. A previous model of the basin based on gravity modeling (Keller et al., 1984) is now obsolete in several areas due to (1) new information on basin-bounding structures; (2) a better understanding of rocks that constitute rift-related deposits; (3) better estimates of physical properties; (4) a better understanding of the geophysical signature of pre-rift and transitional rocks; and (5) more sophisticated approaches to geophysical modeling (Grauch and Keller, 2004; Drenth et al., 2011, 2013; Ruleman et al., 2013; Grauch et al., 2015, 2017; Thompson et al., in press; Turner et al., in press). These more recent concepts, developed locally within or at the edges of the present study area, await integration into a broader synthesis of the geometry and development of the southern San Luis Basin.

This study uses gravity, magnetotelluric, and aeromagnetic geophysical data, along with geologic data and limited subsurface constraints derived from interpreted drill hole logs to interpret the configuration of subbasins and major bounding structures present within the southern San Luis Basin. The main goal of the study is to determine how the Rio Grande rift developed and is currently expressed in the southern San Luis Basin, including the following specific goals: (1) estimate the thickness of rift-related basin-filling sediments; (2) determine what the rift-sediment thickness distribution indicates about basin structure and temporal pattern of rifting; and (3) delineate major rift-bounding structures, many of which are concealed from direct observation.

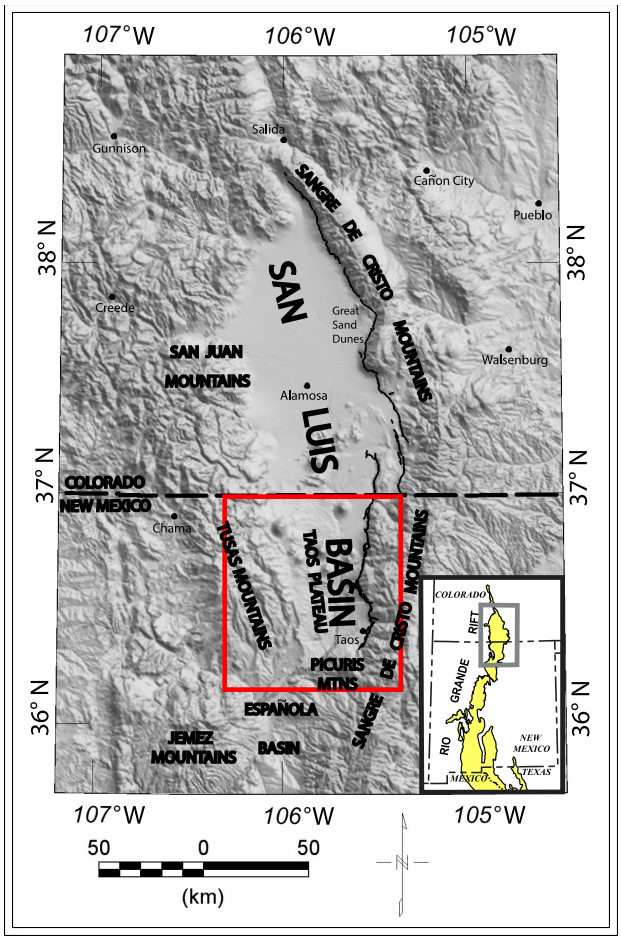


Figure 1. Physiography and geography of the San Luis Basin, Colorado and New Mexico. Red box shows area of this study and area of Figure 2. Sangre de Cristo fault zone shown as heavy black line. Inset map shows location of Figure 1 in relation to the Rio Grande rift (modified from Hudson and Grauch, 2013).

GEOLOGIC BACKGROUND

Tectonic History Overview

Large portions of the San Luis Basin region were uplifted during the Ancestral Rocky Mountain and Laramide orogenies (e.g., Cather, 2004; Kues and Giles, 2004), with erosion removing most preexisting Mesozoic and Paleozoic sedimentary rocks. Subsequent Cenozoic extension associated with the Rio Grande rift occurred along much of the uplifted orogen (Sales, 1983; Kellogg, 1999; Kluth, 2007). Like much of the Southern Rocky Mountains, a significant portion of the San Luis Basin region was covered by middle Tertiary volcanic rocks of the Southern Rocky Mountain volcanic field (SRMVF) (Steven, 1975; Lipman, 2007). The transition from SRMVF magmatic activity to Rio Grande rift subsidence occurred over a period of several million years following Oligocene activity in the San Juan Mountains volcanic locus (Lipman and Mehnert, 1975; Thompson and Machette, 1989; Ingersoll et al., 1990; Thompson et al., 1991; Smith, 2004; Zimmerer and McIntosh, 2012). The Sangre de Cristo Mountains and Sangre de Cristo fault system—major tectonic elements associated with rifting—did not initially form in the southern San Luis Basin area until ~20 Ma or later (Kelley and Duncan, 1986). As with other Rio Grande rift basins, the southern San Luis Basin filled with clastic sediments and some lava flows during Neogene and Quaternary tectonism.

The following sections introduce several geologic units, faults, and previous concepts of basin evolution that are critical to understanding the new interpretations presented here.

Pre-Rift Rocks

Proterozoic rocks crop out in the Sangre de Cristo, Tusas, and Picuris mountains (Fig. 3). Their configuration under the San Luis Basin is largely unknown due to a small number of exposures and few borehole penetrations. Proterozoic rocks in the region include mafic complexes

Downloaded from https://pubs.geoscienceworld.org/uwyo/rmg/article-pdf/54/2/97/4907139/05402097.pdf
by USGS Library, Benjamin Drenth

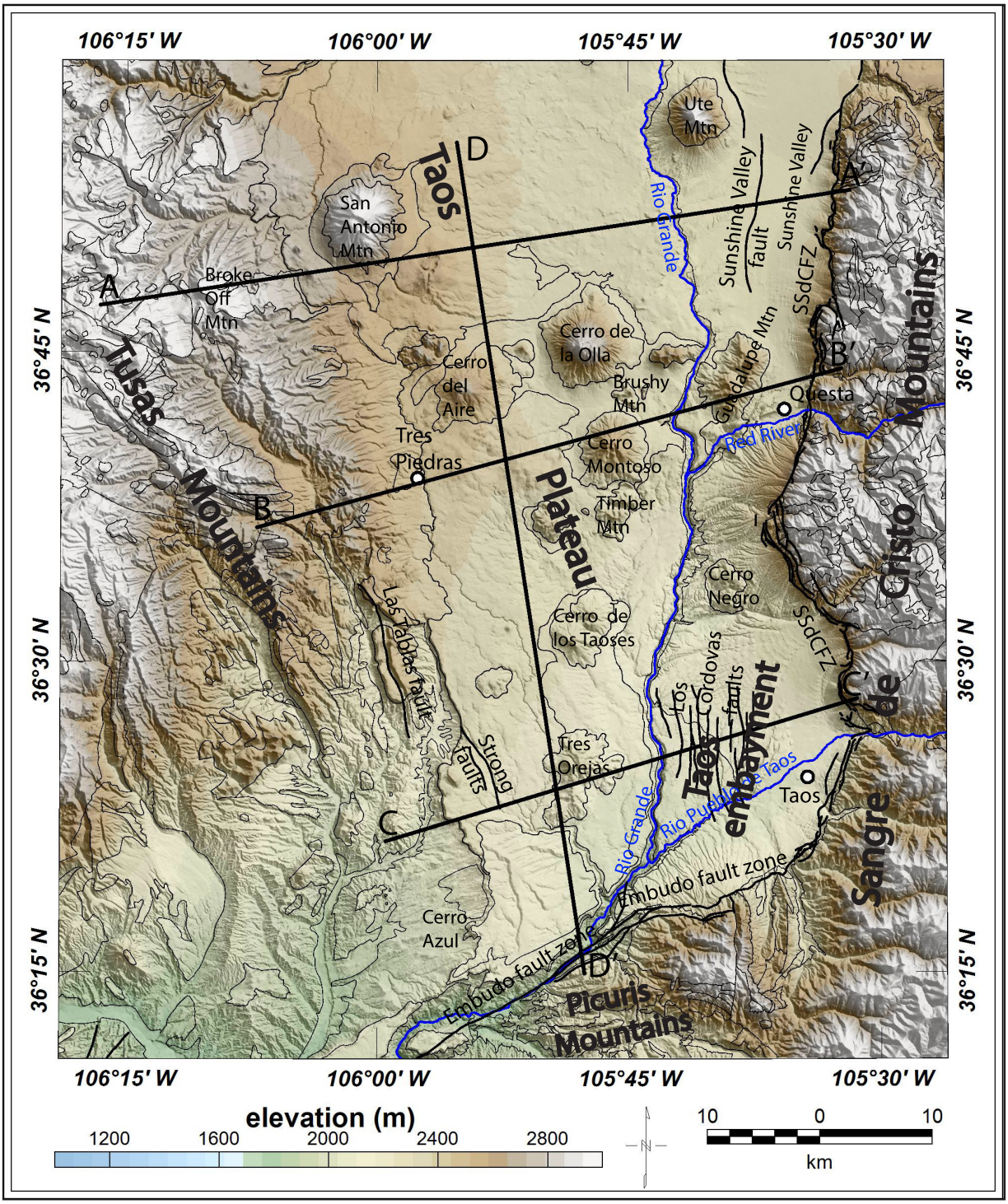


Figure 2. Hillshade digital elevation model showing physiographic features and Quaternary faults of the study area. Features mentioned in the text are labeled. Selected linework from Figure 3 shown for spatial reference. Locations of profile models shown. Quaternary faults located away from the Embudo fault zone are from the U.S. Geological Survey (Quaternary Fault and Fold Database of the United States, 2017). Quaternary faults along the Embudo fault zone from mapping by the New Mexico Bureau of Mines and Mineral Resources (renamed New Mexico Bureau of Geology and Mineral Resources in 2001) (Bauer and Kelson, 1997; Kelson and Bauer, 1998; Bauer et al., 2000; Kelson et al., 2001; Kelson and Bauer, 2003). SSdCFZ: southern Sangre de Cristo fault zone.

Downloaded from https://pubs.geoscienceworld.org/uwyo/rmg/article-pdf/54/2/97/4907139/05402097.pdf
by USGS Library, Benjamin Drenth

(such as the Moppin Complex in the Tusas Mountains), metasedimentary and metavolcanic rocks, and granitic/gneissic plutons (Bauer and Williams, 1989; Williams, 1991; Bauer, 1993; Jones et al., 2009, 2011).

Pre-rift sedimentary rocks crop out in the Paleozoic Taos trough situated in a portion of the Sangre de Cristo Mountains east and southeast of Taos (Baltz and Myers, 1999, and references therein). These consist of mainly fine-grained siliciclastic rocks with minor limestone, and may reach a maximum thickness of ~2 km (Miller et al., 1963). The Paleozoic rocks may extend under the southern San Luis Basin (Baltz and Myers, 1999), although deposition may have been limited or nonexistent west of the Picuris-Pecos fault zone (introduced below) that was active during formation of the Taos trough (Woodward et al., 1999; Bauer et al., 2016). Mesozoic sedimentary rocks crop out in the region (e.g., Thompson et al., 2015), although none are known to exist within the southern San Luis Basin.

The Eocene El Rito Formation, representing erosion from Laramide uplifts (Logsdon, 1981; Maldonado, 2008), primarily crops out in the western Tusas Mountains. Thicknesses as much as 135 m have been mapped in isolated parts of the northeastern Tusas Mountains (Wobus and Manley, 1982; Manley et al., 1987), although these rocks may be part of the Los Pinos Formation (introduced below) (e.g., Aby et al., 2010). The El Rito Formation, and other unknown pre-rift Tertiary sedimentary rocks, may exist under parts of the southern San Luis Basin, particularly near the Tusas Mountains.

Oligocene (SRMVF) magmatism (Steven, 1975; Lipman, 2007) is both pre-rift and transitional (discussed below) in the southern San Luis Basin region. Pre-rift andesitic flows, volcaniclastic deposits, and tuffs from the San Juan Mountains volcanic locus are at least 400 m thick in the northern Tusas Mountains near the state border (Manley, 1982a). However, these rocks thin abruptly to the southeast, with only 20–30 m of tuffs present near the south side of Broke Off Mountain (Manley, 1982b; Wobus and Manley, 1982). The Carpenter Ridge Tuff, dated at 27.73 ± 0.05 Ma (Lipman and Mehnert, 1975; Turner et al., in press), is the youngest tuff of the San Juan Mountains volcanic locus preserved in the southern San Luis Basin region. Other Oligocene volcanic rocks crop out at the Brushy and Timber mountains and form part of a horst of pre-rift rocks that extends in the shallow subsurface northward into southern Colorado (Lipman and Mehnert, 1979; Thompson et al., 1986; Thompson and Schilling, 1988; Thompson and Machette, 1989).

Transitional Rock Units

Late Oligocene to Miocene volcanic and volcaniclastic rocks that record the shift from volcanism and associated sedimentation of the SRMVF to earliest extension-related sedimentation and volcanism are considered transitional rocks, rather than entirely pre-rift or syn-rift deposits. The transition occurred over a period of several million years and overlapped significantly in space and time across the region (e.g., Turner et al., in press). The style, magnitude, and tectonic significance of basin formation and sedimentation during this time are uncertain and subject to debate.

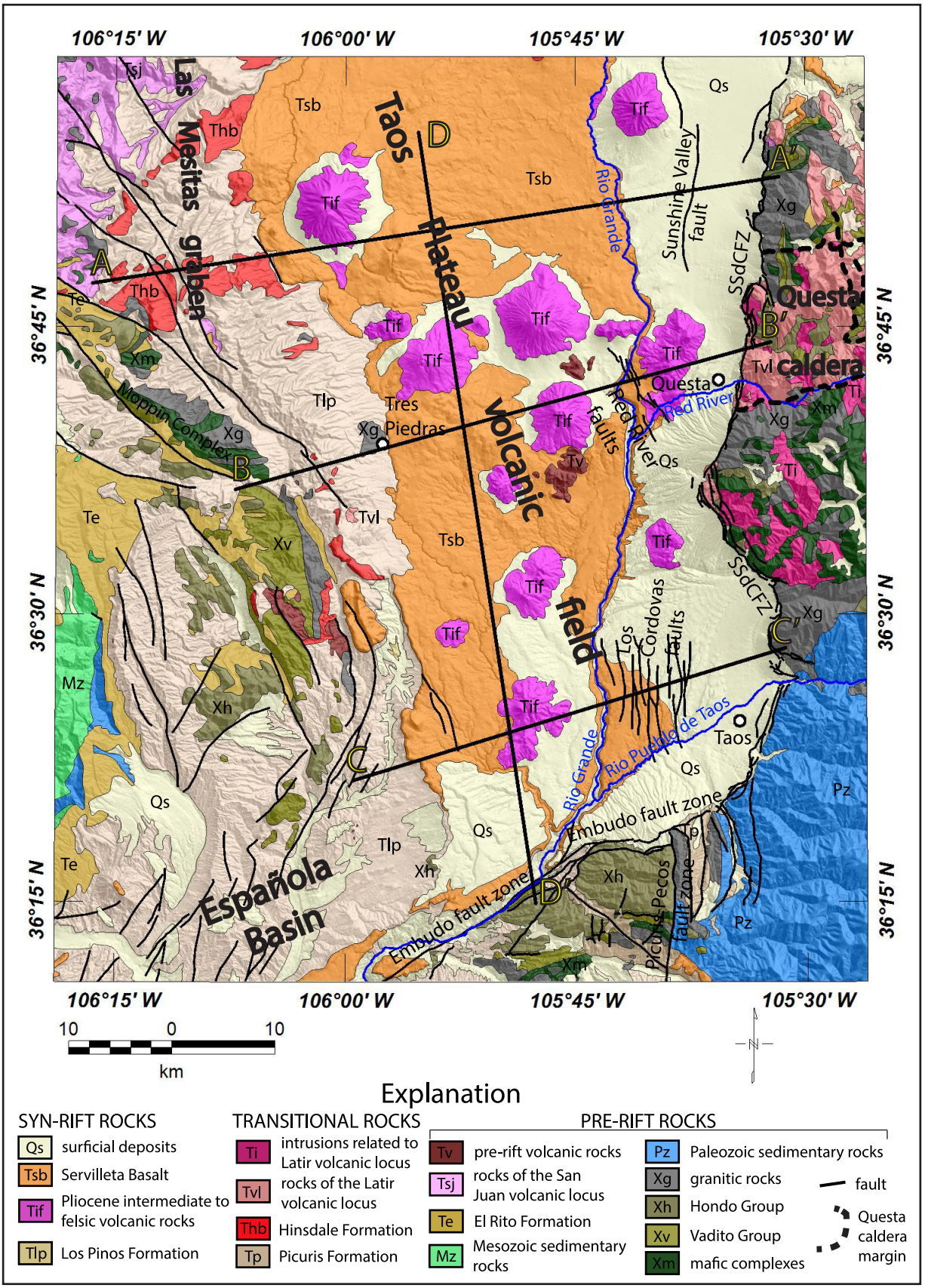
In the Sangre de Cristo Mountains, the Questa caldera of the Latir volcanic locus formed as the ~25.4 Ma Amalia Tuff erupted (Lipman et al., 1986; Lipman and Reed, 1989; Tappa et al., 2011; Zimmerer and McIntosh, 2012). This tuff represents one of the last expressions of SRMVF magmatism across the Southern Rocky Mountains region (Steven, 1975; Lipman, 2007). The mapped boundary of the Questa caldera is truncated by the southern Sangre de Cristo fault zone at the San Luis Basin margin near Questa (Fig. 3), suggesting that the western margin of the caldera lies under the basin (Cordell et al., 1985; Lipman and Reed, 1989). The Amalia Tuff was deposited across much of the region, as indicated by exposures in the Tusas Mountains (e.g., Aby et al., 2010). Distal deposits are less than 100 m thick, and most are much thinner. An upper-crustal silicic batholith formed as part of the Latir volcanic locus and has been interpreted as the source of a gravity low (Fig. 4) over a large part of the Sangre de Cristo Mountains (Cordell et al., 1985; Lipman, 1988).

The Upper Oligocene to Upper Miocene Los Pinos Formation consists of volcaniclastic sediments derived from the San Juan and Latir volcanic loci (Butler, 1946, 1971; Lipman, 1975a, b; Manley, 1981). Locally, the Los Pinos Formation reaches a thickness of 350 m near Broke Off Mountain in the northeast Tusas Mountains (Manley, 1982b). The Los Pinos Formation has been regarded as either an early expression of basin filling (e.g., Lipman and Mehnert, 1975; Chapin and Cather, 1994), or as erosional products local to magmatic centers (Ingersoll et al., 1990; Ingersoll and Cavazza, 1991; Large and Ingersoll, 1997; Ingersoll, 2001; Smith et al., 2002). Interbedded with the Los Pinos Formation are basaltic rocks of the ~26 Ma to ~19 Ma Hinsdale Formation (Lipman, 1975b; Lipman and Mehnert, 1975; Thompson et al., 1991; Thompson and Lipman, 1994).

The > 34.5 Ma to < 18.6 Ma Picuris Formation consists mainly of volcaniclastic sedimentary rocks and records the transition from pre- to early rift sedimentation (Baltz, 1978; Rehder, 1986; Aby et al., 2004; Bauer and Kelson, 2004). The Picuris Formation crops out along the southern margin of the basin near the Embudo fault. Its distribution in the

Figure 3, next page. Simplified geology and physiography of the study area (Bauer and Williams, 1989; Lipman and Reed, 1989; Anderson and Jones, 1994; Green and Jones, 1997; Read et al., 2004; Koning and Mansell, 2011). Locations of profile models shown. SSdCFZ: southern Sangre de Cristo fault zone.

Downloaded from https://pubs.geoscienceworld.org/uwyo/rmg/article-pdf/54/2/97/4907139/05402097.pdf
by USGS Library, Benjamin Drenth



Downloaded from https://pubs.geoscienceworld.org/uwyo/rmg/article-pdf/54/2/97/4907139/05402097.pdf
by USGS Library, Benjamin Drenth

subsurface basinward of the Embudo fault zone is largely unknown, although it may be present at least as far north as the Rio Pueblo de Taos, a tributary of the Rio Grande in New Mexico (Fig. 3) (Bauer et al., 2016; Grauch et al., 2017).

Syn-Rift Rocks

This paper regards that the onset of the Rio Grande rift is related to the establishment of the Sangre de Cristo fault system and the Embudo fault zone. Exposures of early rift deposits are largely either eroded or covered by younger volcanic flows and sedimentary deposits, so estimates on the timing of rift inception have come from estimates on the timing of uplift of the Sangre de Cristo Mountains. Interpretation of apatite fission track data in the study area is complicated by thermal resetting associated with ~25 Ma magmatism of the Latir volcanic locus (Kelley and Duncan, 1986). However, the apatite fission-track data that are considered reliable, combined with similar data from a broader region and regional stratigraphic arguments, suggest that the segment of the Sangre de Cristo Mountains adjacent to the southern San Luis Basin was uplifted sometime after 20 Ma (e.g., Kelley and Duncan, 1986; Smith, 2004).

Syn-rift sediments that accumulated within subsiding basins of the Rio Grande rift are classified as the Santa Fe Group (Spiegel and Baldwin, 1963; Ingersoll et al., 1990; Brister and Gries, 1994; Chapin and Cather, 1994). Although transitional rock units are known to be present within many Rio Grande rift basins, the Santa Fe Group is commonly assumed to be volumetrically dominant, based largely on borehole data and geophysical modeling (e.g., Keller et al., 1984; Brister and Gries, 1994; Kluth and Schaftenaar, 1994; Grauch and Keller, 2004; Drenth et al., 2013).

Interbedded with the uppermost Santa Fe Group sediments are numerous flows of the regionally extensive ~5.2 to 2.9 Ma Servilleta Basalt, the volumetrically dominant unit of the mainly Pliocene Taos Plateau volcanic field (Lipman and Mehnert, 1975, 1979; Dungan et al., 1984, 1989; Appelt, 1998; Read et al., 2004; Cosca et al., 2014; Bauer et al., 2015; Turner et al., 2018; Thompson et al., in press; Turner et al., in press). The flows vary considerably in cumulative thickness, from zero at many outcrops of pre-rift rocks to roughly 200 m in the south-central part of the Taos Plateau, although their thickness is not constrained in most of the study area due to a paucity of drilling. Older, rift-related basalts between the ages of the Hinsdale Formation and Servilleta Basalt are interpreted to be present in the subsurface of the southern San Luis Basin near the town of Taos (Grauch et al., 2017), and are likely present but undetected elsewhere within the basin. Large dacitic volcanic domes and andesitic shield volcanoes of the Taos Plateau volcanic field are less volumetrically significant than the Servilleta Basalt, but form high-relief mountains (Lipman and Mehnert, 1979) and serve as useful landmarks (see Fig. 3). Notable examples include San Antonio Mountain, Ute Mountain, Guadalupe Mountain, Cerro de la Olla, Cerro Montoso, Cerro Negro, and Tres Orejas (e.g., Thompson et al., in press).

Faulting

Numerous faults have been mapped in the southern San Luis Basin and along its margins. Some have demonstrable Quaternary displacement (Personius and Machette, 1984; Machette et al., 1998; Kelson et al., 2004), and are correlated with major basin and intrabasin structural boundaries. Fault segments with Quaternary displacement generally exist along (or near) the eastern and southeast margins of the basin (Quaternary fault and fold database, https://earthquake.usgs.gov/hazards/qfaults/).

The dominantly west-down Sangre de Cristo fault system is the major basin-bounding structure that juxtaposes basin-fill deposits in the hanging wall against the precipitous Sangre de Cristo Mountains. The Sangre de Cristo fault system is divided into northern, central, and southern zones, with the southern zone extending from southern Colorado to the area southeast of Taos, thus forming the eastern margin of the southern San Luis Basin (Figs. 2 and 3) (Personius and Machette, 1984; Menges, 1990; Ruleman and Machette, 2007; Ruleman et al., 2013).

South of Taos, the west-down and generally north-striking southern Sangre de Cristo fault zone changes to a more southwesterly strike and transitions (Bauer and Kelson, 2004) to the Embudo fault zone, a portion of which forms the southeastern margin of the southern San Luis Basin. The Embudo fault zone is up to 9 km wide and includes steeply dipping left-lateral, down-to-northwest oblique slip faults, and represents the transfer zone between the San Luis and Española basins (Muehlberger, 1979; Bauer and Kelson, 1997; Kelson et al., 1997; Kelson and Bauer, 1998; Machette et al., 1998; Bauer et al., 2000; Kelson et al., 2001; Kelson and Bauer, 2003; Bauer and Kelson, 2004; Bauer et al., 2016; Grauch et al., 2017). Faulting started about 18–11 Ma along fault segments now concealed within the basin in the vicinity of the modern Rio Pueblo de Taos, and subsequently migrated southeastward to its current location (Grauch et al., 2017).

The north-striking, strike-slip Picuris-Pecos fault zone intersects the southern Sangre de Cristo fault zone and the Embudo fault zone near their intersection (Fig. 3). The Picuris-Pecos fault zone has a complex slip history (e.g., Bauer and Kelson, 2004; Bauer and Ralser, 1995; Cather et al., 2011 and references therein) that is largely pre-rift, but with at least some activity synchronous with rifting (e.g., Bauer and Kelson, 2004). North of the Embudo fault zone, the syn-rift Los Cordovas faults (Figs. 2 and 3) are mostly

Downloaded from https://pubs.geoscienceworld.org/uwyo/rmg/article-pdf/54/2/97/4907139/05402097.pdf
by USGS Library, Benjamin Drenth

north-striking, west-down normal faults that cut Servilleta Basalt and Santa Fe Group (Personius and Machette, 1984) and may be a northern manifestation of the Picuris-Pecos fault zone (Bauer and Kelson, 2004; Grauch et al., 2004; Bauer et al., 2016; Grauch et al., 2017).

Several intrabasin faults cut the Servilleta Basalt. These include the northeast-down Red River and east-down Sunshine Valley faults (Winograd, 1959; Personius and Machette, 1984; Ruleman et al., 2013; Bauer et al., 2015; Thompson et al., in press). An additional syn-rift structure, the Gorge fault zone, is inferred at different places along the Rio Grande corridor. It corresponds to multiple east-down and west-down, northwest- and northeast-trending scarps between the approximate latitudes of the Guadalupe and Ute mountains (Ruleman et al., 2013; Bauer et al., 2015). That definition of the Gorge fault zone may be consistent with a proposed fault zone along the Rio Grande corridor that extends north from approximately the latitude of Taos (Dungan et al., 1984; Bauer and Kelson, 2004).

Faults along the western margin of the southern San Luis Basin and in the Tusas Mountains locally cut basalts of the Hinsdale Formation, and are dominantly northeast-striking, southwest-down structures (Barker, 1958; Manley, 1982a, b; Manley and Wobus, 1982b; Wobus and Manley, 1982; Manley and Wobus, 1985; Manley et al., 1987; Koning et al., 2007; Aby, 2008; Aby et al., 2010; Turner et al., 2018). The Las Tablas fault (Aby et al., 2010) and the Strong faults (Aby, 2008) may have Quaternary slip. No significant faults are mapped in the immediate vicinity of Cerro Azul at the southwestern margin of the southern San Luis Basin (Figs. 2 and 3; Koning et al., 2016).

Previous Basin Models and Concepts of Evolution

The San Luis Basin can be crudely approximated as a half graben, with the west-down Sangre de Cristo fault system acting as the master fault system on the eastern margin (e.g., Lipman and Mehnert, 1979; Brister and Gries, 1994; Kluth and Schaftenaar, 1994). A strong gravity gradient corresponding to the southern Sangre de Cristo fault zone reflects the abrupt westward thickening of the basin fill (Cordell, 1978; Cordell and Keller, 1984; Keller et al., 1984; Cordell et al., 1985; Bauer and Kelson, 2004; Grauch and Keller, 2004). Gravity lows associated with the eastern part of the basin (Fig. 4) are attributed to thick accumulations of low-density, rift-related sediments in a north–south trending set of subbasins immediately west of the southern Sangre de Cristo fault zone. The western margin of this set of subbasins has traditionally been conceptualized as an east-down fault zone corresponding to a large gravity gradient subparallel to the Rio Grande (Fig. 4) and lies along the eastern margin of the horst of pre-rift Oligocene volcanic rocks at Brushy and Timber mountains (Cordell, 1978; Lipman and Mehnert, 1979; Cordell and Grauch, 1985; Grauch and Keller, 2004). The location and sense of motion of the east-down fault zone are largely consistent with concepts of the Gorge fault zone developed by others (Dungan et al., 1984; Bauer and Kelson, 2004; Grauch and Keller, 2004; Ruleman et al., 2013; Thompson et al., in press). In that model, the portion of the basin west of the horst is dramatically shallower than the portion to the east, with an abrupt separation formed by the east-down fault zone and horst (e.g., Lipman and Mehnert, 1979). However, another concept of basin geometry infers a more gradual shallowing of the basin west of the east-down fault zone and horst (Keller et al., 1984; Grauch and Keller, 2004). In this alternate view, a prominent northeast-trending gravity gradient west of the Rio Grande, the Olla-King gravity gradient (Fig. 4) of Grauch and Keller (2004), is produced by an east-down fault zone at the western basin boundary.

Sediment thickness estimates for the southern San Luis Basin are widely divergent. Early thickness estimates for the subbasins immediately west of the southern Sangre de Cristo fault zone were > 5 km, with thicknesses of < 300 m present west of the Rio Grande corridor and the horst of pre-rift Oligocene volcanic rocks (Lipman and Mehnert, 1979). The 3D gravity model of Keller et al. (1984) estimated thicknesses as large as ~4 km near the southern Sangre de Cristo fault zone adjacent to the western edge of the Questa caldera, and a more gradual westward thinning toward the basin-bounding structure inferred at the location of the Olla-King gravity gradient (Grauch and Keller, 2004). More recent modeling suggests low-density sediment thicknesses of ~1.2 km in Sunshine Valley (Ruleman et al., 2013), < 1 km near the western edge of the Questa caldera (Bauer et al., 2015; Grauch et al., 2015), and ~1.8 km a short distance northwest of Taos (Grauch et al., 2017). In the vicinity of the southern Sangre de Cristo fault zone-Embudo fault zone transition, the modeled thickest part of the basin lies 5–7 km west of the southern Sangre de Cristo Mountains fault zone (Grauch et al., 2017). At Sunshine Valley and near Questa, the thickest sediment accumulations are interpreted to lie directly adjacent to the range front fault zone. The different pattern in the Taos embayment was interpreted as evidence of a post 6 Ma southeastward shift of the southern Sangre de Cristo fault zone to its present position; prior to 6 Ma the master faults of the Taos subbasin were located 5–10 km basinward of the present-day range front (Grauch et al., 2017).

Other parts of the southern San Luis Basin have historically received less attention, particularly those along the western basin margins. A gravity low in the area of Tres Orejas mountain (Grauch and Keller, 2004) was interpreted to reflect a 2- to 2.5-km-thick accumulation of low-density sediments (Keller et al., 1984). The gravity low may be caused by a rift-related subbasin, by a pre-rift Tertiary basin, or by a northwestern prong of the Paleozoic Taos trough (Baltz and Myers, 1999; Grauch and Keller, 2004). The latter scenario would require that significant thicknesses of Paleozoic sediments

Downloaded from https://pubs.geoscienceworld.org/uwyo/rmg/article-pdf/54/2/97/4907139/05402097.pdf
by USGS Library, Benjamin Drenth

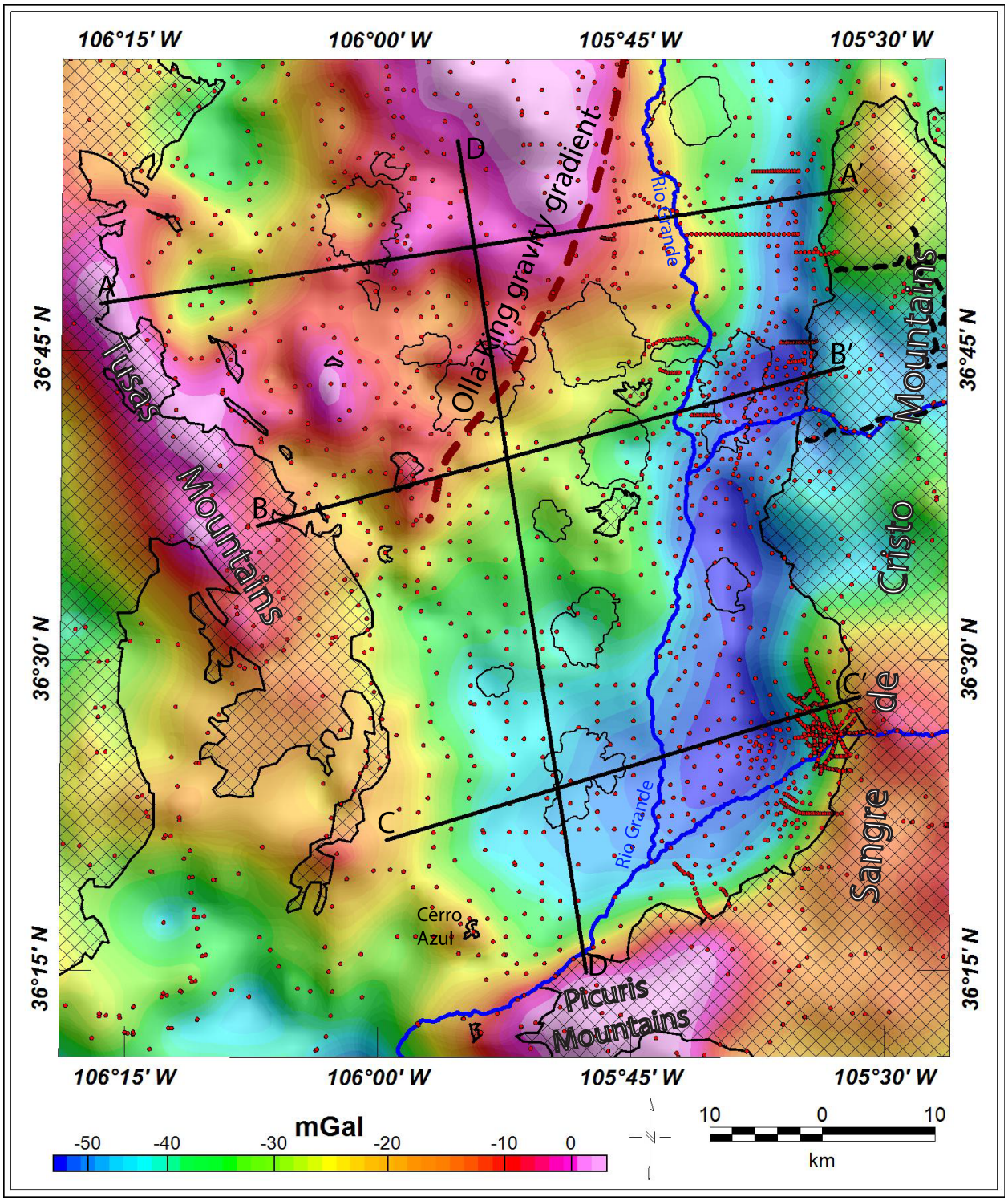


Figure 4. Isostatic residual gravity anomalies, interpolated onto a 1-km grid. Warm colors indicate higher densities (highs); cool colors indicate lower densities (lows). Red dots are gravity station locations. Selected linework from Figure 3 shown for spatial reference. Locations of profile models shown. Hachured pattern indicates areas where pre-rift rocks crop out. Dashed red line indicates Olla-King gravity gradient of Grauch and Keller (2004).

Downloaded from https://pubs.geoscienceworld.org/uwyo/rmg/article-pdf/54/2/97/4907139/05402097.pdf
by USGS Library, Benjamin Drenth

accumulated west of the Picuris-Pecos fault zone (Grauch and Keller, 2004). Other gravity lows in the northeastern Tusas Mountains have been attributed to the Broke Off Mountain subbasin of Drenth et al. (2011), currently regarded as the southern part of the rift-transitional Las Mesitas graben (Turner et al., in press). Preliminary gravity modeling yielded an estimated thickness of > 900 m of Los Pinos Formation, and the subbasin boundaries were interpreted to be largely fault controlled (Drenth et al., 2011, 2013).

The southwestern margin of the southern San Luis Basin is formed by a largely buried northwest-trending structural high that produces a gravity high (Fig. 4) and separates the San Luis Basin from the Española Basin to the southwest (Cordell, 1978; Kelley, 1978; Cordell, 1979; Keller et al., 1984; Grauch and Keller, 2004; Koning et al., 2004; Koning et al., 2016). Proterozoic rocks crop out at Cerro Azul, the only surface expression of the structural high. Major basin-bounding faults in this area are not exposed, likely concealed by Servilleta Basalt (Koning et al., 2004).

GEOPHYSICAL DATA AND METHODS

Geophysical analysis for this study is based primarily upon quantitative, 3D modeling of gravity data, although magnetotelluric and aeromagnetic data also provide important perspectives on the interpretations of basin geometry and evolution.

Gravity Data

Gravity anomalies reflect lateral variations of density. Gravity highs occur over regions of relatively high densities, such as mountains composed of crystalline basement, and places where low-density sediments are thin or absent. Gravity lows occur over large volumes of low-density materials, such as unconsolidated sediments. Generally large density contrasts between low-density rift-filling sediments (such as the Santa Fe Group) and older rocks (Table 1) make gravity data useful for defining the configuration of basins within the Rio Grande rift (e.g., Cordell, 1978; Keller et al., 1984; Grauch and Connell, 2013).

Regional quality (1–5 km station spacing) gravity data were extracted from the PACES gravity database maintained by the University of Texas at El Paso (Pan-American Center for Earth and Environmental Studies, 2006) and supplemented with the acquisition of about 600 new gravity stations in the southern San Luis Basin from 2006 through 2015 (Drenth, 2016). Standard techniques (e.g., Blakely, 1995) and a density of 2,670 kg/m^3 (Hinze, 2003) were used to process the data to complete Bouguer anomalies. Isostatic residual gravity anomalies, representing density variations within the upper crust (Simpson et al., 1986), were calculated using the isostatic regional model of Heywood (1992). The results are interpolated on a 1-km grid (Fig. 4).

3D Gravity Modeling

A previous 3D gravity model of the San Luis Basin (Keller et al., 1984) facilitated mapping of major tectonic elements and thickness of the Santa Fe Group. That work, however, assumed a single density contrast (350 kg/m^3) between the Santa Fe Group and older rocks, and had limited data in several key areas where new data have since been acquired.

We use a more sophisticated approach to determine basin geometry: a 3D inverse method that separates the estimated gravitational field of low-density, largely rift-related sediments from the estimated field due to older, denser rocks (Table 1) (Jachens and Moring, 1990; Blakely and Jachens, 1991; Blakely, 1995; Grauch and Connell, 2013). To accomplish this separation, the method adheres to independent constraints on geology and basin-fill thickness, and incorporates a user-defined density-depth function to invert the estimated field due to low-density basin fill for thickness. The depths computed in this fashion are based on densities (2,170 kg/m^3 above a depth of 1.25 km; 2,350 kg/m^3 below a depth of 1.25 km) relative to an assumed background value of 2,670 kg/m^3. The density-depth function used for the inversion is based on density logs for similar rift-fill sediment in the Albuquerque Basin (Grauch and Connell, 2013). Boreholes in the southern San Luis Basin lack similar density logs, but based on their similar geologic settings we assume that the Albuquerque Basin densities are valid in the southern San Luis Basin.

Important advantages of this 3D inversion method are that it (1) honors geologic map constraints, including locations of exposed pre-rift rocks at basin boundaries and inside the basin; (2) honors constraints from the few drill holes that reach pre-rift rocks; (3) allows the density of pre-rift rocks to vary, by varying the estimated field due to pre-rift rocks as needed to satisfy independent geologic constraints; and (4) accommodates basin geometries in 3D. This method, however, has some important limitations as well: (1) abrupt thickness variations at basin and subbasin boundaries are smoothed; (2) thicknesses may be underestimated in areas where basalts are present in a basin; and (3) gravity data coverage is insufficient at most of the large volcanoes (Fig. 4) to locally interpret major basin and subbasin boundaries. The inversion is based on a grid with 1-km grid cell resolution, and abrupt thickness variations across basin- and subbasin-bounding structures, such as normal faults, appear as sloping surfaces. Major structural boundaries are easily identifiable, but characteristics such as their dip and presence of single or multiple faults are not resolvable in the inversion results.

The presence of basalt causes thickness to be underestimated because the basalts are significantly denser than the surrounding sediments in the basin, reducing the amplitudes of gravity lows. For example, the underestimate of low-density basin-fill thickness may exceed 100 m for an area with a 200-m thickness of interbedded basalt (the expected worst-

Downloaded from https://pubs.geoscienceworld.org/uwyo/rmg/article-pdf/54/2/97/4907139/05402097.pdf
by USGS Library, Benjamin Drenth

Table 1 (p. 56–57). Geophysical properties of geologic units in the study area.

Unit	Density (kg/m^3)	Density reference	Estimated resistivity range (ohm-m)	Resistivity reference
Tif at Guadalupe Mountain	2,450	Grauch et al., 2015	Assumed 50–500 (dry)	N/A
Servilleta Basalt (Tsb)	~2,670	Proprietary sonic log near Taos; Ruleman et al., 2013	Assumed 20–500 (dry)	N/A
Santa Fe Group (Tsf) and Los Pinos Formation (Tlp), upper 1.25 km depth	2,170	Grauch and Connell, 2013	Assumed 2–50 (wet)	Rodriguez and Sawyer, 2013
Santa Fe Group (Tsf) and Los Pinos Formation (Tlp), 1.25–2.75 km depth	2,350	Grauch and Connell, 2013	Assumed 2–50 (wet)	Rodriguez and Sawyer, 2013
Hinsdale Formation (assumed massive basalt) (Thb)	2,625	Grauch and Drenth, 2016	Assumed similar to Servilleta Basalt	N/A
Picuris Formation (Tp)	2,250	Grauch et al., 2017	Assumed similar to Santa Fe Group	N/A

case scenario). Attempts to model the gravitational effect of the basalts and remove that effect prior to the inversion led to even greater uncertainties, mainly because the distribution of basalt at depth in the basin is not well known due to a lack of adequate boreholes.

Results from the 3D gravity inversion include an estimated gravity map due to effects of pre-rift rocks (Fig. 5), estimated thickness distribution of low-density basin fill (Fig. 5), and estimated structural elevation on the base of the low-density basin fill (Fig. 6) computed by subtracting the thickness distribution from a smoothed version of the surface topography. Constraints on the depth to the bottom of the low-density basin fill for the inversion (Fig. 5) come from mapped locations of older rocks (places where the low-density basin-fill thickness is zero and gravity stations directly sample the effects of pre-rift rocks) (Manley, 1982b; Manley and Wobus, 1982a, b; Wobus and Manley, 1982; Thompson and Schilling, 1988; Anderson and Jones, 1994; Green and Jones, 1997).

The estimated thickness distribution of low-density basin fill is only an approximation of the thickness of syn-rift units, because certain pre-rift and transitional units have similar densities to the Santa Fe Group (Table 1). Strictly speaking, the estimated thickness of low-density basin fill represents the combined thickness of the transitional Picuris Formation, Los Pinos Formation, and Amalia Tuff, in addi-

Downloaded from https://pubs.geoscienceworld.org/uwyo/rmg/article-pdf/54/2/97/4907139/05402097.pdf
by USGS Library, Benjamin Drenth

Table 1 (continued). Geophysical properties of geologic units in the study area.

Unit	Density (kg/m^3)	Density reference	Estimated resistivity range (ohm-m)	Resistivity reference
Tuffs of San Juan volcanic locus and Amalia Tuff (Tsj & Tvl, respectively)	Assumed ~2,000–2,300	Drenth et al., 2012, and references therein	unknown	N/A
Paleozoic clastic rocks (Pz)	2,540	Grauch and Drenth, 2016; Grauch et al., 2017	2–23 (wet)	Rodriguez and Sawyer, 2013
Paleozoic limestones (Pz)	2,670	Grauch and Drenth, 2016; Grauch et al., 2017	25–41	Rodriguez and Sawyer, 2013
Granitic rocks (Xg)	2,600	Grauch and Drenth, 2016	> 600	Rodriguez and Sawyer, 2013
Hondo Group (Xh)	2,690	Grauch and Drenth, 2016	Assumed 50–500 (dry)	N/A
Vadito Group (Xv)	2,700	Grauch and Drenth, 2016	Assumed 50–500 (dry)	N/A
Mafic complexes (Xm)	~2,900	Grauch and Drenth, 2016; Grauch et al., 2017	Assumed ~100 and greater	N/A

tion to the volumetrically dominant Santa Fe Group itself. Additional complications may arise from the undetected presence of tuffs from the San Juan volcanic locus (low density, but presumed small thickness) and/or the El Rito Formation (unknown density and unknown thickness). For those reasons, the gravity inversion may overestimate the thickness of the syn-rift sediments. This overestimate of syn-rift thickness is likely balanced to some extent by the underestimate due to the effects of intrabasin basalt, although the paucity of subsurface geologic constraints makes the degree of any balancing impossible to estimate quantitatively.

The 3D inversion results have additional uncertainties. A major source of uncertainty is the lack of independent constraints (i.e., outcrops of pre-rift rocks, and boreholes that reach the base of the low-density basin fill) on thickness across large areas (Fig. 5). The 3D modeling results are most reliable near areas with intrabasin constraints, and areas near the basin margins where the gravitational effects of pre-rift rocks are relatively well constrained. Another possible source of uncertainty is that the densities assumed valid for the low-density basin fill may be inaccurate in some places. In the context of the 3D model results, these

Downloaded from https://pubs.geoscienceworld.org/uwyo/rmg/article-pdf/54/2/97/4907139/05402097.pdf
by USGS Library, Benjamin Drenth

issues are manifested as quantitative uncertainty on the estimated thickness of the low-density basin fill. In places lacking independent constraints, that total uncertainty could be in the small hundreds of meters, locally approaching the total estimated thickness of low-density basin fill in thinner parts of the basin. However, the interpreted geometry of the basin, meaning the presence of subbasins and major bounding structures, is considered qualitatively robust despite the quantitative ambiguities.

2D Gravity Modeling

A series of 2D models (Figs. 7–10) illustrate several details of the 3D interpretation in cross-section form. The estimated gravitational effects of low-density basin fill (not shown in map form) are modeled to illustrate the interpreted basin geometry in relation to pre-rift rocks, basin- and subbasin-bounding structures, and other geophysical interpretations (introduced below). The estimated gravitational effects of pre-rift rocks are not modeled beyond the 3D approach described above. The detailed extent of sediments interbedded with basalts cannot be shown at the regional scale of this modeling. Instead, the thickness of basalt indicated by the models is consistent with the total thickness of basalt measured in borehole logs in places where such constraints exist.

Magnetotelluric Data and Methods

Electromagnetic geophysical methods detect variations in the electrical properties of rocks, in particular electrical resistivity or its inverse, electrical conductivity. In the upper crust, the electrical resistivity of geologic units largely depends on their fluid content, porosity, fracture density, temperature, and state of alteration, as well as the presence of conductive minerals, such as clay, graphitic carbon, and metallic minerals (e.g., Keller and Frischknecht, 1966; Hearst and Nelson, 1985; Keller, 1987; Palacky, 1987; Nelson and Anderson, 1992; Hallenburg, 1998; Hearst et al., 2000). Fresh-water-saturated, unconsolidated, terrestrial, alluvial sediments are commonly conductive to moderately conductive (2–70 ohm-m). Sediments containing conglomerate and coarse, clean sand possess higher electrical resistivities (tens of ohm-m, e.g., Deszcz-Pan et al., 2000); silty sand and siltstone have lower values of resistivity (less than 10 ohm-m), and clay-rich rocks commonly have even lower resistivities. Unaltered, little fractured igneous rocks and metamorphic rocks are normally highly resistive and typically possess resistivity values of a few hundred to thousands of ohm-m.

The magnetotelluric (MT) method is a passive, ground-based electromagnetic geophysical technique that investigates the distribution of electrical resistivity below the surface at depths of tens of meters to tens of kilometers (Vozoff, 1991). It does so by measuring Earth's natural electric and magnetic fields, with worldwide lightning activity and geomagnetic micropulsations providing the energy and main frequency bands. The MT method has been used successfully to help define basin geometry in the Albuquerque and Española basins (e.g., Rodriguez and Sawyer, 2013).

Thirty-five MT soundings along three profiles were acquired between 2009 and 2011 in the study area (Fig. 6) (Ailes and Rodriguez, 2010, 2015). The data are inverted for resistivity structure using unconstrained 2D inversions that correspond roughly in location to parts of three of the 2D gravity models (Figs. 7–10). Given significant ambiguities involved in both methods, the gravity modeling was not used to constrain the MT modeling, nor was the MT modeling used to constrain the gravity modeling. Thus, the MT models are independent of the 3D gravity model. Estimated resistivity values used for interpretations in the southern San Luis Basin are listed in Table 1. Further details of the MT method, data collection, data processing, and inversion methodology are given in Appendix 1 (also see Ailes and Rodriguez, 2010, 2015).

Magnetic Data and Methods

Magnetic anomalies reflect spatial variations of total magnetization, the vector sum of induced and remanent magnetizations (e.g., Blakely, 1995; Hinze et al., 2013). Induced magnetization is proportional to magnetic susceptibility and has the same direction as the present-day ambient field. Remanent magnetization, a long-lived property, may be directed in a different direction than the induced magnetization. Volcanic rocks normally carry large-magnitude components of remanent magnetization (e.g., Reynolds et al., 1990; Clark, 1997). The magnetizations of unconsolidated sediments and sedimentary rocks are usually much lower than those of volcanic and intrusive rocks. In this region, volcanic rocks, such as the Servilleta Basalt (e.g., Brown et al., 1993), are the dominant sources of large-amplitude magnetic anomalies.

Total-field aeromagnetic data used in part of this study area were acquired by three high-resolution (200–400 m flight line spacing, 100–150 m above the ground) surveys acquired during 2003–2005 (Bankey et al., 2004, 2005, 2006). The data were analytically continued to a surface 100 m above the ground and merged with existing data (Kucks et al., 2001) to create an aeromagnetic map of the study area. A reduction-to-pole transformation—a standard geophysical technique to center anomalies over their sources (Baranov and Naudy, 1964; Blakely, 1995)—was applied to the aeromagnetic data using the ambient field inclination of 64 degrees and declination of 10 degrees (our Figs. 6 and 11A).

Aeromagnetic data are not included in the 2D modeling (Figs. 7–10) because the aeromagnetic anomalies are dominated by the under-constrained effects of the distribution and physical properties of the Servilleta Basalt. These include the thickness and total magnetization intensity of individ-

Downloaded from https://pubs.geoscienceworld.org/uwyo/rmg/article-pdf/54/2/97/4907139/05402097.pdf
by USGS Library, Benjamin Drenth

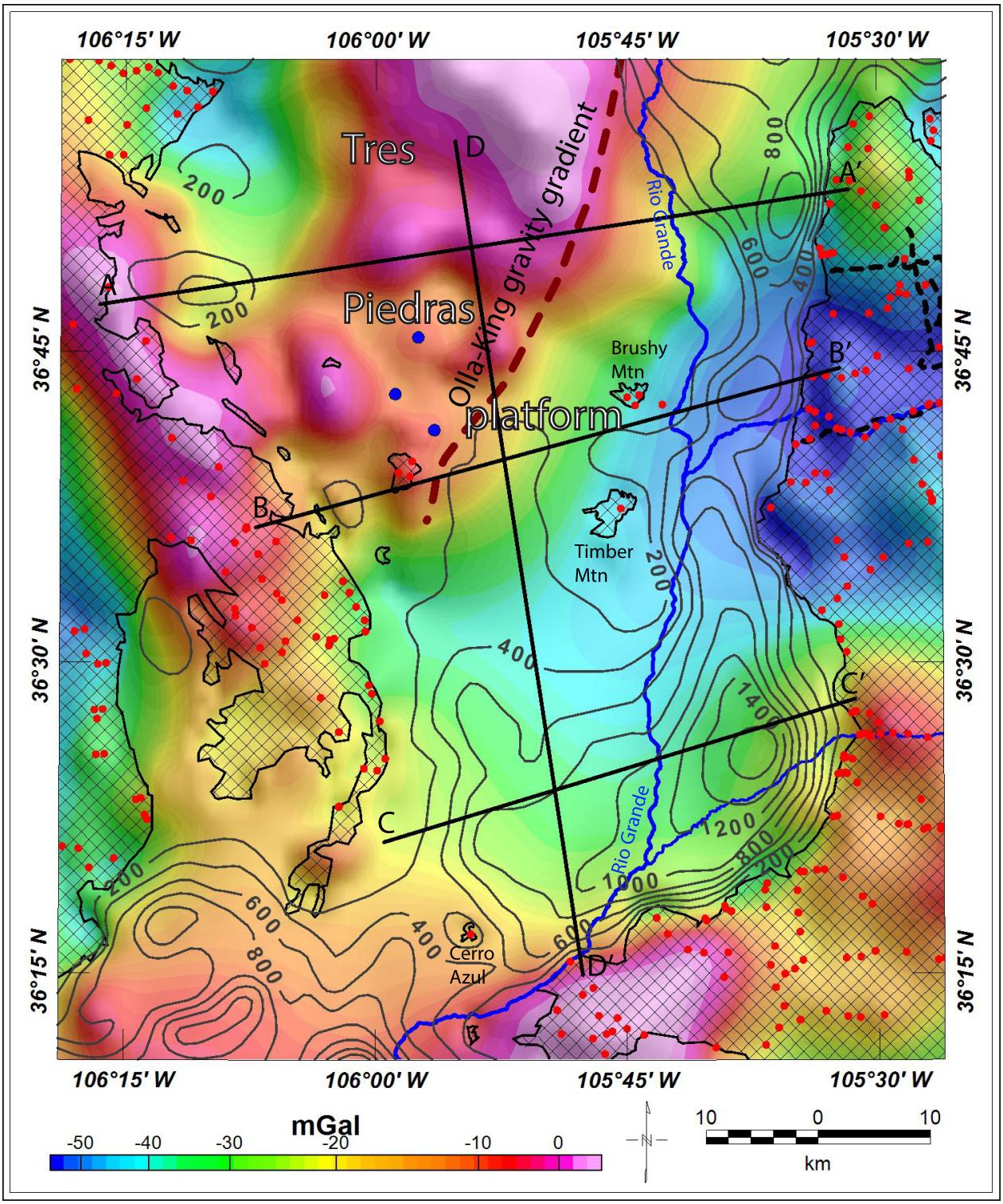


Figure 5. 3D gravity inversion constraints and results. Colors represent estimated gravitational effect of pre-rift rocks. Hachured areas indicate pre-rift rocks, both exterior and interior to the basin. Red dots are gravity stations located on pre-rift rocks. Blue dots are wells that penetrate pre-rift rocks. Gray contours are estimated thickness of low-density basin fill, 200-m contour interval. Selected linework from Figure 3 shown for spatial reference. Locations of profile models shown. Dashed red line indicates Olla-King gravity gradient of Grauch and Keller (2004).

Downloaded from https://pubs.geoscienceworld.org/uwyo/rmg/article-pdf/54/2/97/4907139/05402097.pdf
by USGS Library, Benjamin Drenth

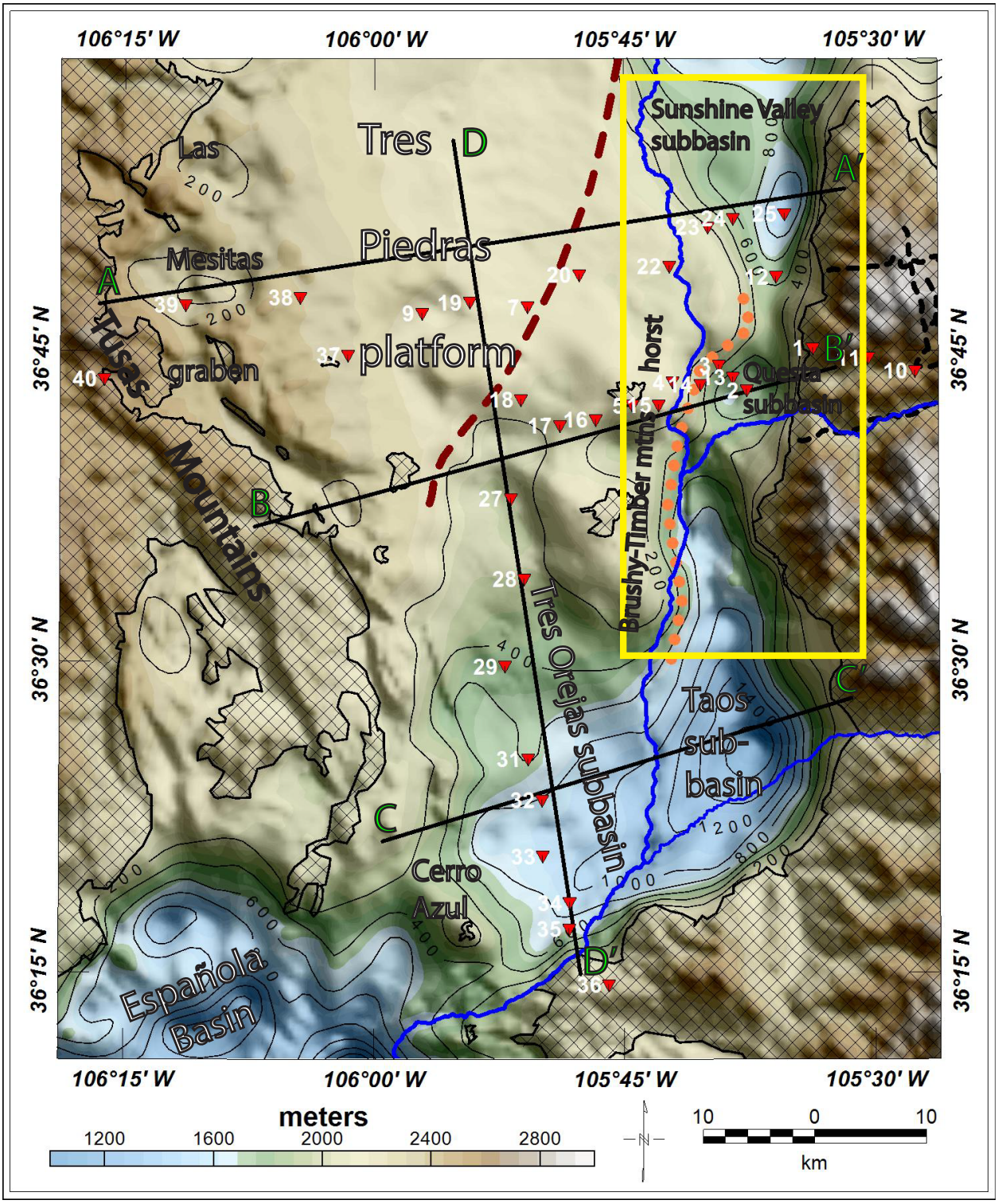


Figure 6. Estimated structural elevation at the base of basin fill, computed by subtracting the estimated low-density basin-fill thickness from the surface elevation. Hachured areas indicate exposed pre-rift rocks, both exterior and interior to the basin. Gray contours are estimated thickness of low-density basin fill, 200-m contour interval. Dotted orange line indicates the location of the Gorge fault zone as interpreted in this study. Dashed red line indicates Olla-King gravity gradient of Grauch and Keller (2004). Locations of the 35 magnetotelluric (MT) soundings shown by red triangles. Selected linework from Figure 3 shown for spatial reference. Locations of profile models shown. Yellow rectangle shows area of Figure 11.

Downloaded from https://pubs.geoscienceworld.org/uwyo/rmg/article-pdf/54/2/97/4907139/05402097.pdf
by USGS Library, Benjamin Drenth

ual flows, differences in remanent magnetization polarity between different stacked flows, and the numbers of stacked flows in different places. Quantitative modeling of the aeromagnetic data is highly sensitive to changes in any of those largely unconstrained details. The aeromagnetic data can be fit in the 2D profile modeling by choosing as few as one of those variables to adjust, but that approach would be arbitrary and would not lead to geologically meaningful conclusions. Instead, joint gravity and aeromagnetic models are presented for selected locations where the aeromagnetic data help establish concepts related to basin formation (Figs. 11 and 12).

INTERPRETATIONS

The major conclusion is that the southern San Luis Basin is strongly compartmentalized and contains a series of subbasins that are separated from each other by major structural highs and fault zones (Fig. 6). The eastern basin margin is well defined by the southern Sangre de Cristo fault zone, consistent with previous models; however, several other major tectonic elements are shown differently than in previous models. Subbasins and major grabens are here identified by gravity lows that are interpreted to be caused by accumulations of low-density basin fill estimated at least 200 m thick. Where available, the MT inversions help define subbasins by showing areas interpreted to contain conductive (2–50 ohm-m) basin fill. Subbasin boundaries are interpreted in places where the estimated thickness of low-density and conductive basin fill changes rapidly over short distances. Structural highs are interpreted in places with relatively thin to nonexistent cover of low-density basin fill (estimated thicknesses < 200 in 3D gravity model).

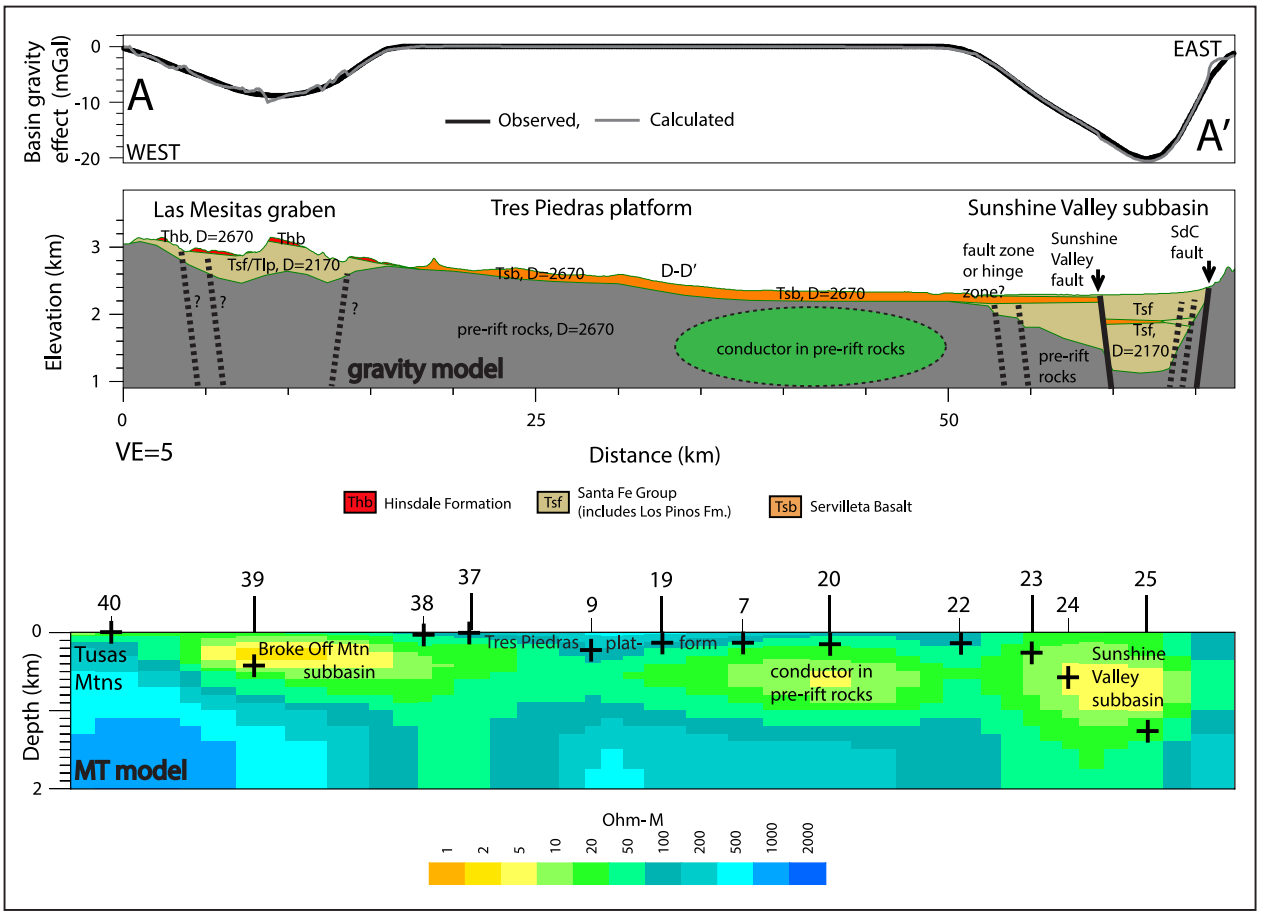


Figure 7. Geophysical profiles and models along A-A′. Top panel: estimated gravitational effect of low-density basin fill ("Observed") and calculated model response. Middle panel: geologic model expressed in terms of densities and geologic concepts. Densities (D) in kg/m^3. Sangre de Cristo fault zone (SdC fault) and Sunshine Valley fault shown as solid lines; other interpreted faults shown as dashed lines. Bottom panel: approximately co-located resistivity model resulting from 2D inversions of magnetotelluric (MT) data. MT station numbers listed above the model. Refer to Figure 6 for station and profile locations. Black crosses indicate the structural elevation at the base of the low-density basin fill estimated from the 3D gravity modeling (Fig. 6) under each MT station.

Downloaded from https://pubs.geoscienceworld.org/uwyo/rmg/article-pdf/54/2/97/4907139/05402097.pdf
by USGS Library, Benjamin Drenth

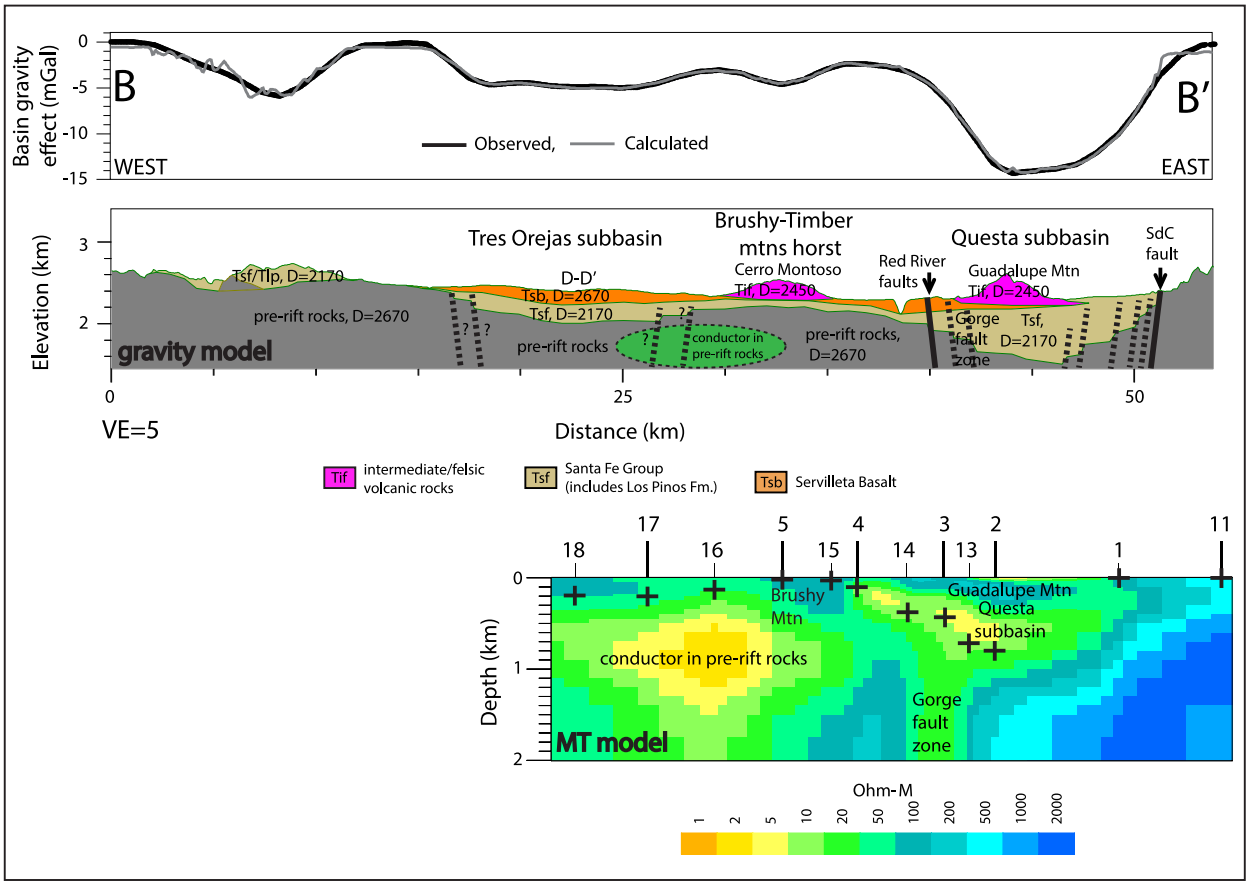


Figure 8. Geophysical profiles and models along B-B′. Top panel: estimated gravitational effect of low-density basin fill ("Observed") and calculated model response. Middle panel: geologic model expressed in terms of densities and geologic concepts. Densities (D) in kg/m^3. Sangre de Cristo fault zone (SdC fault) and Red River faults shown by solid lines; other interpreted faults shown as dashed lines. Bottom panel: approximately co-located resistivity model resulting from 2D inversions of magnetotelluric (MT) data. MT station numbers listed above the model. Refer to Figure 6 for station and profile locations. Black crosses indicate the structural elevation at the base of the low-density basin fill estimated from the 3D gravity modeling (Fig. 6) under each MT station.

Las Mesitas Graben

The structural low formerly called the Broke Off Mountain subbasin (Drenth et al., 2011) is now understood to be a southern portion of the Las Mesitas graben of Turner et al. (in press) in the northwestern part of the study area (Fig. 6). It contains a significant thickness of the Los Pinos Formation, locally capped by ~26 Ma basalts of the Hinsdale Formation (Turner et al., 2018, in press), and is thus regarded as a feature that predates syn-rift formation of the broader southern San Luis Basin.

The Las Mesitas graben is modeled as having up to a ~400 m thickness of Los Pinos Formation in the Broke Off Mountain area, a result consistent with both gravity and MT models (Figs. 6 and 7), and an exposed thickness of ~350 m (Manley, 1982b). This estimate is considered more reliable than an earlier thickness estimate of > 900 m (Drenth et al., 2011), due to an improved understanding of the surface geology in the area (Turner et al., 2018) and the associated constraints placed on the 3D gravity model. The new estimate is also consistent with the independent MT modeling, and is considered to be a more geologically realistic thickness estimate for the Los Pinos Formation. It is possible that other geologic units, such as volcanic rocks of the San Juan volcanic locus and the El Rito Formation, are present within the Broke Off Mountain subbasin (Drenth et al., 2011). The similarity of the ~400-m thickness estimate to the exposed Los Pinos Formation thickness (~350 m) suggests that older geologic units are either volumetrically minor within the graben, or that they underlie the graben as it is expressed in the 3D gravity model.

Based on geologic mapping and stratigraphic studies (Turner et al., 2018., in press) and modeled low-density basin-fill thicknesses that locally reach 200 m or greater (this study), the Las Mesitas graben extends northward into

Downloaded from https://pubs.geoscienceworld.org/uwyo/rmg/article-pdf/54/2/97/4907139/05402097.pdf
by USGS Library, Benjamin Drenth

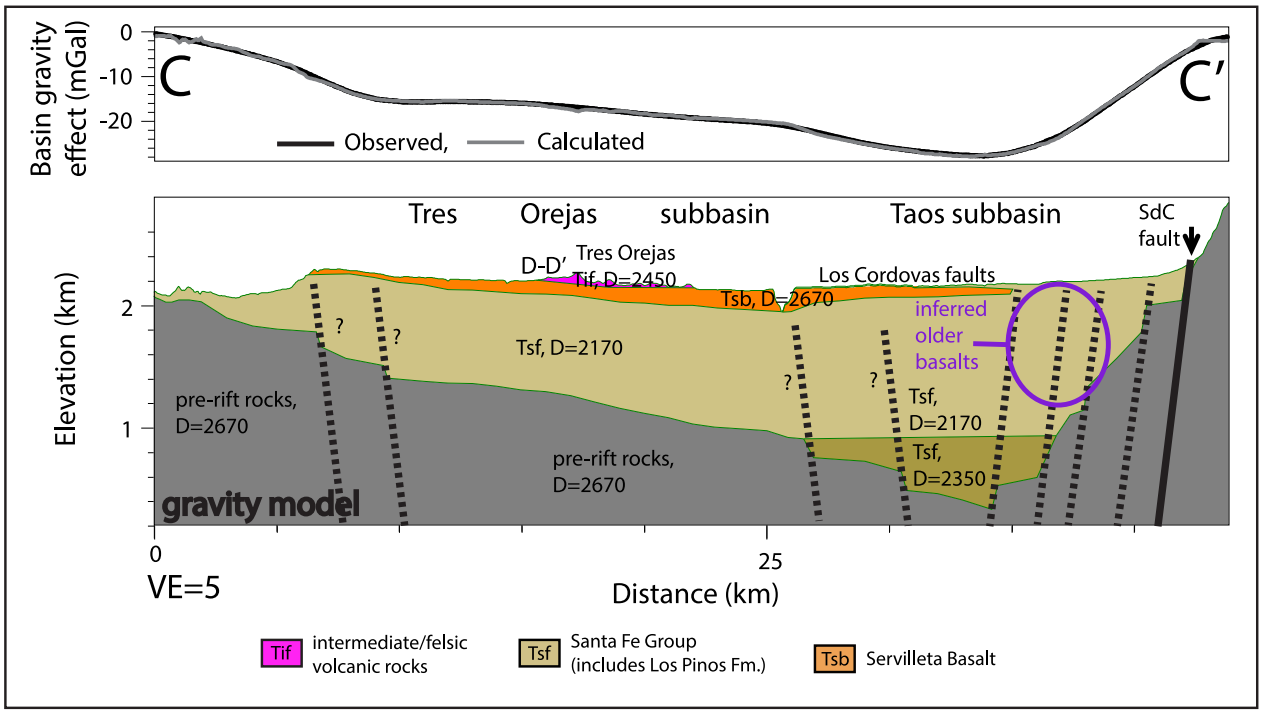


Figure 9. Geophysical profiles and models along C-C′. Top panel: estimated gravitational effect of low-density basin fill ("Observed") and calculated model response. Lower panel: geologic model expressed in terms of densities and geologic concepts. Densities (D) in kg/m^3. Sangre de Cristo fault zone (SdC fault) shown as solid line; other interpreted faults shown as dashed lines. The eastern truncation of the Servilleta Basalt is consistent with the interpretation of Grauch et al. (2017). The purple oval shows the area hypothesized by Grauch et al. (2017) to contain basalts older than the Servilleta Basalt.

southern Colorado, where it deepens to ~1 km (Drenth et al., 2013). The subbasin extends approximately 30 km to the southeast of Broke Off Mountain as a series of shallow structural lows (mainly < 200 m thick), where it ends at a structural high separating it from the Tres Orejas subbasin (Fig. 6). The exposure of rocks of the Latir volcanic locus at the structural high (Figs. 3 and 6) suggests that pre-rift rocks are locally close to the surface. The structural high also connects with Proterozoic granite that crops out near the community of Tres Piedras (Figs. 3 and 6).

The structural margins of the Las Mesitas graben are difficult to interpret, due to generally poor exposures of faults and lack of data on timing of slip (Drenth et al., 2011), the coarse resolution of the gravity data and modeling, and ambiguities in the interpretation of aeromagnetic lineaments over the basalts of the Hinsdale Formation (Drenth et al., 2011). Several aeromagnetic lineaments may correspond with faults that controlled the subbasin geometry (Drenth et al., 2011).

Tres Piedras Platform and Brushy-Timber Mountain Horst

The 3D gravity model images the Tres Piedras platform as a large area with thin to nonexistent (< 200 m) accumulations of low-density basin fill, and the Servilleta Basalt may lie directly on pre-rift rocks over most of this area (Figs. 6–8, 10). The 3D gravity model shows a small thickness (~200 m) of low-density basin fill between the Brushy and Timber mountains, but this is likely an artifact of a gravity low produced by Cerro Montoso that has no relationship to sedimentary basin fill. The structurally high platform, previously called the Taos Plateau structural high (Drenth et al., 2013), extends into southern Colorado where pre-rift rocks are exposed in the San Luis Hills (Thompson et al., 1986, 1991; Drenth et al., 2013) and likely connects to the Alamosa horst in the subsurface in the northern San Luis Basin (Brister and Gries, 1994; Kluth and Schaftenaar, 1994). The eastern margin crudely follows the Rio Grande corridor and Gorge fault zone (discussed below). The pre-rift volcanic rocks at the Brushy and Timber mountains are interpreted to form a southeastern extension of the Tres Piedras platform that separates the Tres Orejas subbasin on the west from the Taos and Questa subbasins on the east. The extent of the Tres Piedras platform and Brushy-Timber mountains' horst interpreted here is significantly larger than an area modeled by Keller et al. (1984), and more closely matches the model of Lipman and Mehnert (1979) in that the platform has a small thickness (< 200 m) of basin fill.

Downloaded from https://pubs.geoscienceworld.org/uwyo/rmg/article-pdf/54/2/97/4907139/05402097.pdf
by USGS Library, Benjamin Drenth

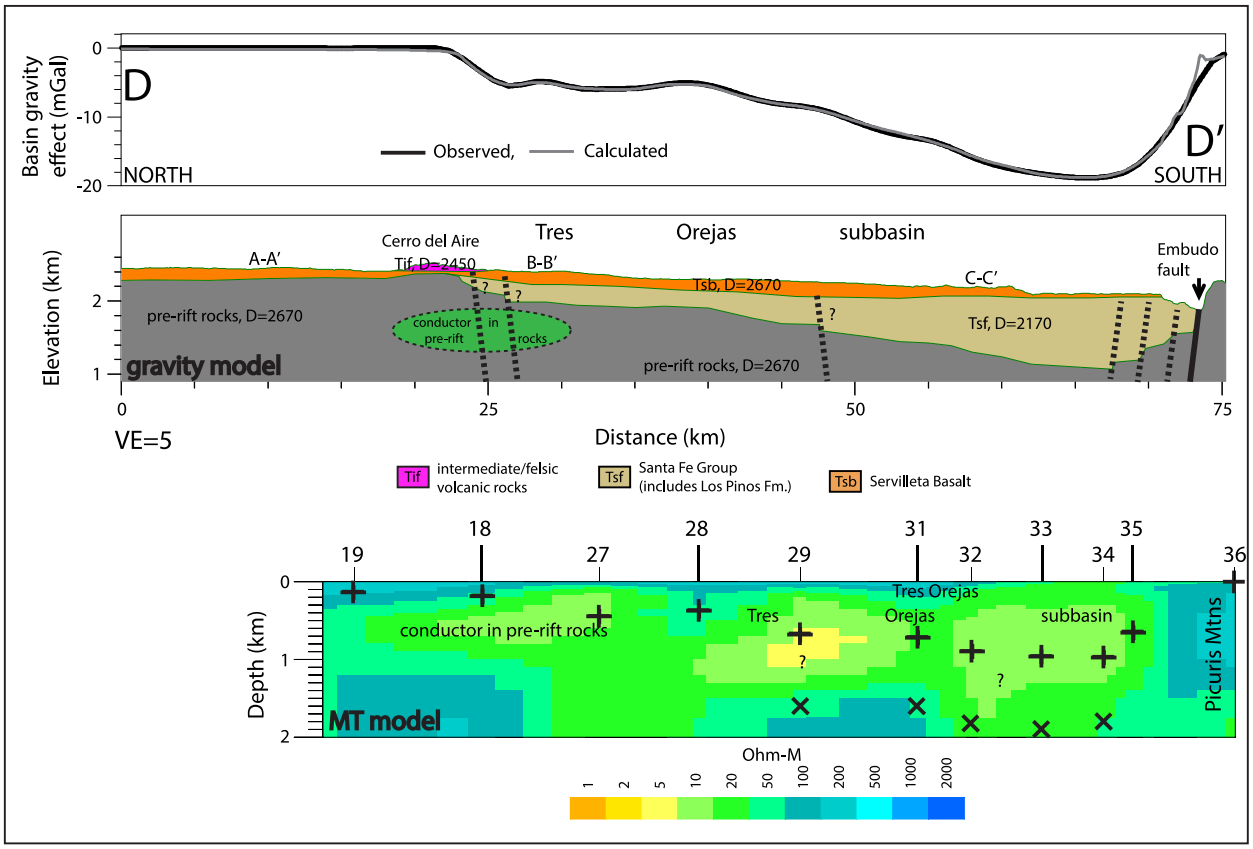


Figure 10. Geophysical profiles and models along D-D′. Top panel: estimated gravitational effect of low-density basin fill ("Observed") and calculated model response. Middle panel: geologic model expressed in terms of densities and geologic concepts. Densities (D) in kg/m^3. Embudo fault zone shown as a solid line; other interpreted faults shown as dashed lines. Bottom panel: approximately co-located resistivity model resulting from 2D inversions of magnetotelluric (MT) data. MT station numbers listed above the model. Refer to Figure 6 for station and profile locations. Black crosses indicate the structural elevation at the base of the low-density basin fill estimated from the 3D gravity modeling (Fig. 6) under each MT station. Rotated black crosses under selected MT stations indicate the structural elevation at the base of the low-density basin fill for an assumed density of 2,350 kg/m^3 (see text).

Dense, pre-rift rocks are interpreted to underlie most of the Tres Piedras platform, apart from the Brushy-Timber mountains' horst area (Fig. 5). Gravity highs due to pre-rift rocks extend west to exposures of Proterozoic rocks in the Tusas Mountains, where the Moppin Complex includes anomalously dense mafic rocks (Table 1) that produce a gravity high (Figs. 2 and 4). No other pre-rift rock units are known to have similarly high densities (Grauch and Drenth, 2016). Dense, mafic Proterozoic rocks, perhaps related to or similar to the Moppin Complex, are thus interpreted to extend in the subsurface northeast of the Tusas Mountains and far to the north, across the Colorado border and well into the central San Luis Basin (Drenth et al., 2013). The Olla-King gravity gradient of Grauch and Keller (2004) is interpreted to represent a pre-rift density boundary, the eastern edge of the dense Moppin Complex-like rocks, and not a major basin- or subbasin-bounding structure (Figs. 4–6). Alternatively, the dense pre-rift rocks may be related to other events. For example, they may represent mafic roots of SRMVF magmatism.

MT modeling shows different aspects of the subsurface of the Tres Piedras platform than does the gravity modeling. The Servilleta Basalt is imaged as a resistor (100–500 ohm-m) reaching a thickness of as much as ~300 m (Figs. 7 and 8), a result consistent with limited deep drilling in the area. However, significantly conductive (5–50 ohm-m) rocks are imaged at greater depths, reaching depths that may exceed 1 km (Figs. 7 and 8). The conductive rocks are interpreted as lying within the pre-rift section, due to their modeled extent beneath resistive pre-rift volcanic rocks at Brushy Mountain (Fig. 8 and Appendix 1). The geologic source of the conductive rocks is unknown, as the low resistivities are atypical for pre-rift rocks. Possible explanations for conductive material contained within pre-rift rocks include a sedi-

Downloaded from https://pubs.geoscienceworld.org/uwyo/rmg/article-pdf/54/2/97/4907139/05402097.pdf
by USGS Library, Benjamin Drenth

mentary basin (Proterozoic, Paleozoic, or Mesozoic), a large volume of hydrothermally altered rocks of unknown age, or brines. The basin explanation is consistent with an interpretation for conductive pre-rift rocks that underlie the San Luis Hills, a short distance north of the Colorado border (Drenth et al., 2013). Alternatively, a hydrothermal alteration explanation is supported by a previous study in the nearby Latir volcanic locus where altered volcanic rocks display low resistivities and have a similar estimated thickness in the Sangre de Cristo Mountains (Long, 1985). Water wells in the Taos Plateau do not provide evidence for brines (Johnson and Bauer, 2012), but the presence of brines at greater depths than penetrated by wells is possible.

Tres Orejas Subbasin

The Tres Orejas subbasin is imaged as a crudely south plunging structural low between the southeastern Tusas Mountains on the west, the Brushy-Timber mountains' horst and Taos subbasin on the east, and the Cerro Azul basement high and Embudo fault zone on the south (Fig. 6). The thickness is estimated from the 3D gravity inversion to increase from north to south, with a maximum thickness approaching 1 km near the Embudo fault zone (Figs. 6, 8–10). This estimate is thinner than a previous maximum thickness estimate of > 2 km (Keller et al., 1984).

The independent gravity and MT models differ significantly in thickness estimates for the Tres Orejas subbasin. Relatively low resistivities (5–20 ohm-m) modeled from the MT data, which are elsewhere consistent with low-density basin fill, extend to depths greater than 1 km for much of the subbasin, with the southern area approaching a thickness of perhaps ~2 km (Fig. 10, note area between station 29 and the Picuris Mountains). The 3D gravity model has no intrabasin constraints over the entire area of the subbasin, and the misfit may be due to that lack of independent control alone. An alternate possibility is that the densities used to model the subbasin are incorrect. For example, the subbasin may contain a significant thickness of Paleozoic and/or pre-rift Tertiary sedimentary rocks, a hypothesis raised by previous workers (Baltz and Myers, 1999; Grauch and Keller, 2004). If present, these pre-rift rocks would not be properly accounted for in the 3D gravity modeling because they have higher densities (2,540 kg/m^3 for Paleozoic clastic rocks; 2,420 kg/m^3 (Grauch and Connell, 2013) for Oligocene sediments) than the low-density basin fill, and their higher densities would be consistent with a thicker subbasin. Such pre-rift rocks may also be relatively conductive. The 3D gravity model was tested with these higher densities, appropriate for Paleozoic or Oligocene rocks, to see if the resulting increased subbasin thickness matched the maximum ~2 km subbasin thickness estimated from the MT modeling. In each case, the results (not shown) indicate a subbasin with a thickness much greater than 2 km, indicating that the Tres Orejas subbasin cannot be entirely explained as a Paleozoic or pre-rift Tertiary feature. However, modeling the subbasin thickness with a density of 2,350 kg/m^3 provides a good fit to the MT-derived thickness estimate. This density is consistent with Miocene (i.e., relatively early syn-rift) basin-fill sediments elsewhere in northern New Mexico (e.g., Grauch et al., 2009; Grauch and Connell, 2013). While the presence of some Paleozoic and pre-rift Tertiary rocks underlying the low-density basin fill cannot be ruled out, this modeling result suggests that the Tres Orejas subbasin is mainly filled with Miocene sediments, and that its true thickness is closer to the MT-derived estimate than to the thickness estimated in the 3D gravity model (Figs. 6 and 10).

Other observations along the southern margin of the Tres Orejas subbasin are consistent with a largely Miocene age. Deepening of the subbasin toward the Embudo fault zone, which initially formed during the Miocene, suggests that the fault zone was active during subbasin formation. Further, the thickest accumulation of low-density basin fill is modeled to lie ~7 km northward of the current trace of the Embudo fault zone (Fig. 10), suggesting that most of the subbasin formed prior to the late Miocene to Pleistocene southeastward shift (Grauch et al., 2017) of the fault zone. As with previous models of the southern San Luis Basin, the 3D gravity model supports that the southwestern margin is formed by the structural high extending northwest and southeast from Cerro Azul. Faults that controlled this margin are not exposed and are presumably covered by the largely Pliocene Servilleta Basalt (Koning et al., 2004), indicating that the margin had largely developed its present geometry by the end of the Pliocene, perhaps even by the end of the Miocene.

The details of other structural margins of the Tres Orejas subbasin are more difficult to interpret, due to generally poor exposures of faults and lack of data on timing of slip, the rather coarse resolution of the gravity data and modeling, and ambiguities in the interpretation of aeromagnetic lineaments (not shown) over the Servilleta Basalt. There is little evidence from geologic mapping for major basinward-stepping normal faults that control the northern and western subbasin margins (e.g., Koning et al., 2007; Aby, 2008; Aby et al., 2010). The western margin of the subbasin is aligned with the southward projection of the Olla-King gravity gradient and may also correspond in location and northward strike of the Tusas-Picuris fault zone, a concealed, pre-rift fault zone hypothesized from regional geophysical data, but not confirmed to exist (Karlstrom and Daniel, 1993; Daniel et al., 1995; Cather et al., 2006). This raises the possibility that a pre-rift structure was reactivated as an east-down fault zone during subbasin formation. The southeast margin of the Tres Orejas subbasin is difficult to distinguish (see Fig. 9) from the Taos subbasin (introduced below), suggesting that the Taos subbasin is partly superimposed on that portion of the Tres Orejas subbasin.

Downloaded from https://pubs.geoscienceworld.org/uwyo/rmg/article-pdf/54/2/97/4907139/05402097.pdf
by USGS Library, Benjamin Drenth

Gorge Fault Zone

The eastern margins of the Tres Piedras platform and Brushy-Timber mountains' horst are formed by the Gorge fault zone, an east-down structural boundary that crudely follows the course of the modern Rio Grande for ~30 km (Figs. 6–9, 11). East of this boundary, a series of north–south trending subbasins are mainly controlled by the southern Sangre de Cristo fault zone. The Gorge fault zone is interpreted as an east-down set of structures that is mainly consistent with the location hypothesized by several previous workers along various parts of its length (Cordell, 1978; Lipman and Mehnert, 1979; Cordell and Keller, 1984; Keller et al., 1984; Cordell et al., 1985; Bauer and Kelson, 2004; Grauch and Keller, 2004; Ruleman et al., 2013; Thompson et al., in press). A new interpretation is that the northern part of this fault zone extends ~6 km east of the Rio Grande at the structural high separating the Questa and Sunshine Valley subbasins (also see Thompson et al., in press). The north end of the fault zone matches the location and trend of the east-down Quaternary Sunshine Valley fault (Figs. 6 and 11), suggesting that the latter is a relatively young expression of deformation along the broader Gorge fault trend. On its south end, displacement on the Gorge fault zone appears to die out along the southeastern margin of the Brushy-Timber mountains' horst.

The Gorge fault zone forms parts of the western margins of the Sunshine Valley, Questa, and Taos subbasins, indicating that, along with the southern Sangre de Cristo fault zone, it partly controlled formation of the subbasins. However, whereas small fault scarps are locally observed (Ruleman et al., 2013), there are no major offsets (i.e., large enough to be reflected in the 3D gravity model) of the Pliocene Taos Plateau volcanic field rocks along the length of the Gorge fault zone. This indicates that it ceased to be a major rift subbasin-forming structure by the end of the Pliocene, with the exception of the Quaternary slip along the Sunshine Valley fault (see below).

The MT modeling indicates a relatively narrow, vertically extensive conductive zone under the gravity-defined Gorge fault zone on profile B-B' (Fig. 8). This electrical signature is notably different than that for surrounding pre-rift rocks and may be explained by anomalous physical properties caused by altered rocks within the fault zone itself. Alternatively, the MT data may be imaging alteration more directly related to volcanic rocks of the Taos Plateau volcanic field, including Guadalupe Mountain, or perhaps the conductive material is related to that imaged under the Tres Piedras platform interpreted to be within pre-rift rocks.

Local Aeromagnetic Expression of Volcanic Rocks

The Taos Plateau volcanic field is dominated volumetrically and spatially by the Servilleta Basalt, the source of the "busy" short wavelength aeromagnetic anomaly patterns (Fig. 11A–B) relevant to understanding certain aspects of subbasin structure. This interpretation is supported by (1) exposures of the Servilleta Basalt in comparison to aeromagnetic anomalies; (2) its strong magnetization (Brown et al., 1993; Grauch et al., 2017); and (3) its presence and absence in shallow wells that match differences in aeromagnetic patterns (Grauch and Keller, 2004; Grauch et al., 2017). Based on comparisons to topographic features and paleomagnetic measurements, areas with generally positive anomalies over the Servilleta Basalt are interpreted (Grauch et al., 2017) to reflect a stack of basalt flows with an overall normal remanent magnetic polarity (i.e., reverse polarity flows may be present, but their effects are outweighed by normal polarity flows). Areas with generally negative anomalies are interpreted to reflect a stack of flows with overall reverse polarity. Areas of smooth aeromagnetic anomalies are interpreted as places where the Servilleta Basalt is either absent or buried deeply.

Large dacitic volcanic domes and andesitic shield volcanoes produce large aeromagnetic anomalies (Fig. 11A–B) that are dominated by the effects of remanent magnetization polarity. The combination of strong remanent magnetizations and high topography allows straightforward interpretations of magnetic polarity to be made (Grauch and Keller, 2004). For example, Ute Mountain and Cerro Negro produce strong negative aeromagnetic anomalies (Fig. 11A–B), meaning that those volcanoes must carry mainly reverse polarity. Guadalupe Mountain has masses of both normal (in the south) and reverse (in the north) polarity rocks, indicating that it formed in two episodes that spanned at least one shift in magnetic polarity (Bauer et al., 2015; Grauch et al., 2015; Thompson et al., in press).

Sunshine Valley Subbasin

The Sunshine Valley subbasin is imaged as a structural depression that widens from ~5 km at its southern boundary to ~20 km at the Colorado border (Figs. 1 and 6). North of the state border (not shown), the structural depression continues to widen, and the Sunshine Valley subbasin is considered to be continuous with the (informally named) Costilla Plains structural depression of Drenth et al. (2013) (also see Ruleman et al., 2013). Interpreted thicknesses in New Mexico are as much as 1.2 km based on both gravity and MT models (Figs. 6 and 7). This maximum thickness is significantly less than the ~3 km previously estimated (Keller et al., 1984). The dominant subbasin-forming structure is the southern Sangre de Cristo fault zone at the eastern margin, as indicated by the location of the greatest thickness of low-density basin fill and greatest structural offset of pre-rift rocks (Figs. 6 and 7).

The western subbasin margin is expressed as a set of structures with much less structural relief than the eastern

Downloaded from https://pubs.geoscienceworld.org/uwyo/rmg/article-pdf/54/2/97/4907139/05402097.pdf
by USGS Library, Benjamin Drenth

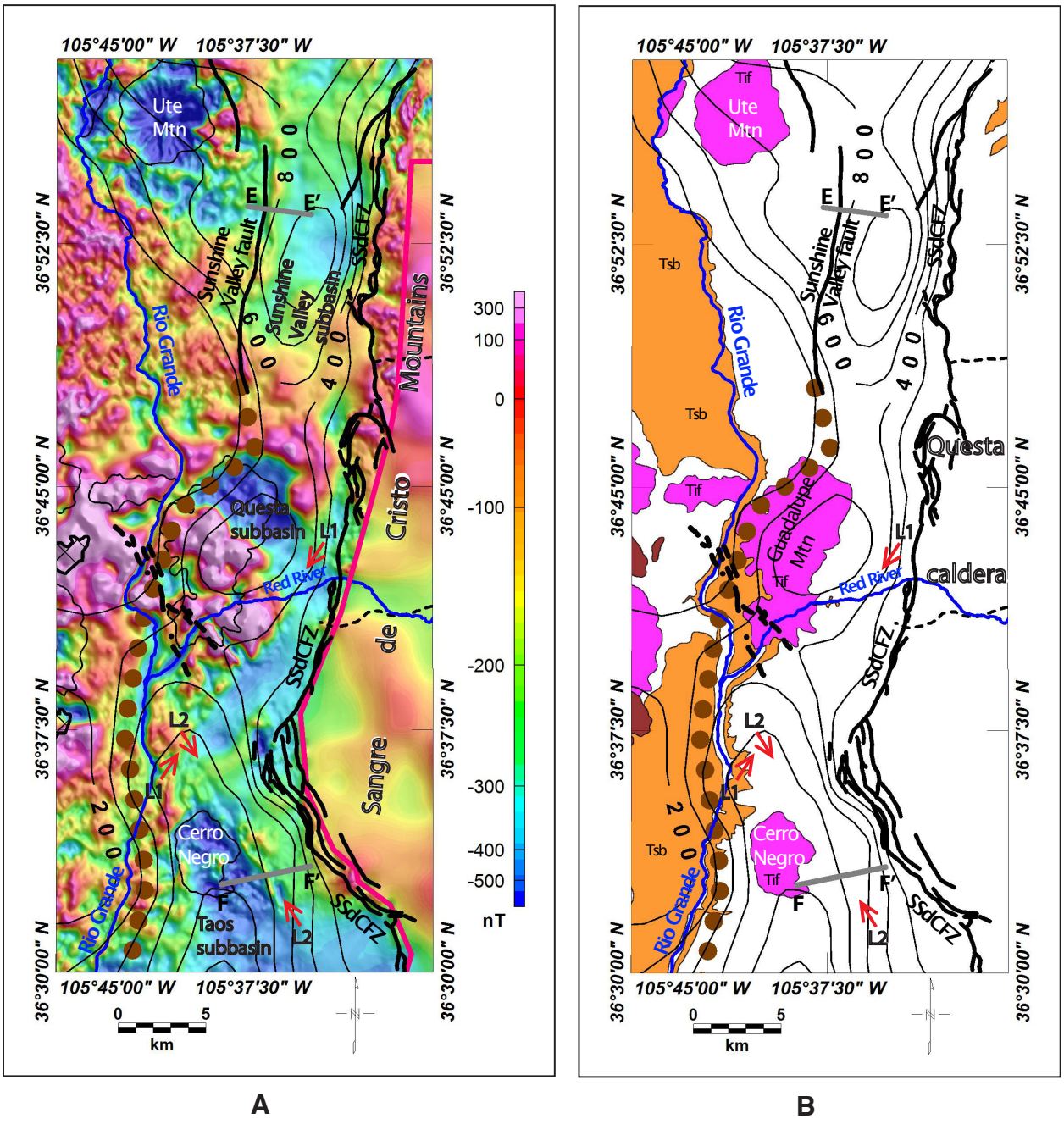


Figure 11. A, Reduced-to-pole aeromagnetic anomalies and summary of tectonic elements in the northern Taos subbasin, Questa subbasin, and Sunshine Valley subbasin region. Selected linework from Figure 6 shown for reference. Location of profile models E-E′ and F-F′ shown. Red arrows show locations and trends of lineaments L1 and L2, discussed in main paper. Pink line shows boundary of high-resolution aeromagnetic data. Black contours are estimated thickness of low-density basin fill, 200-m contour interval. Dotted brown line indicates the location of the Gorge fault zone as interpreted in this study. Solid black lines show Quaternary faults; dashed black lines show Red River faults. SSdCFZ: southern Sangre de Cristo fault zone. **B**, Same as Figure 11A, with aeromagnetic anomalies removed and selected geologic units added from Figure 3. Tsb: Servilleta Basalt; Tif: Pliocene intermediate to felsic volcanic rocks.

Downloaded from https://pubs.geoscienceworld.org/uwyo/rmg/article-pdf/54/2/97/4907139/05402097.pdf
by USGS Library, Benjamin Drenth

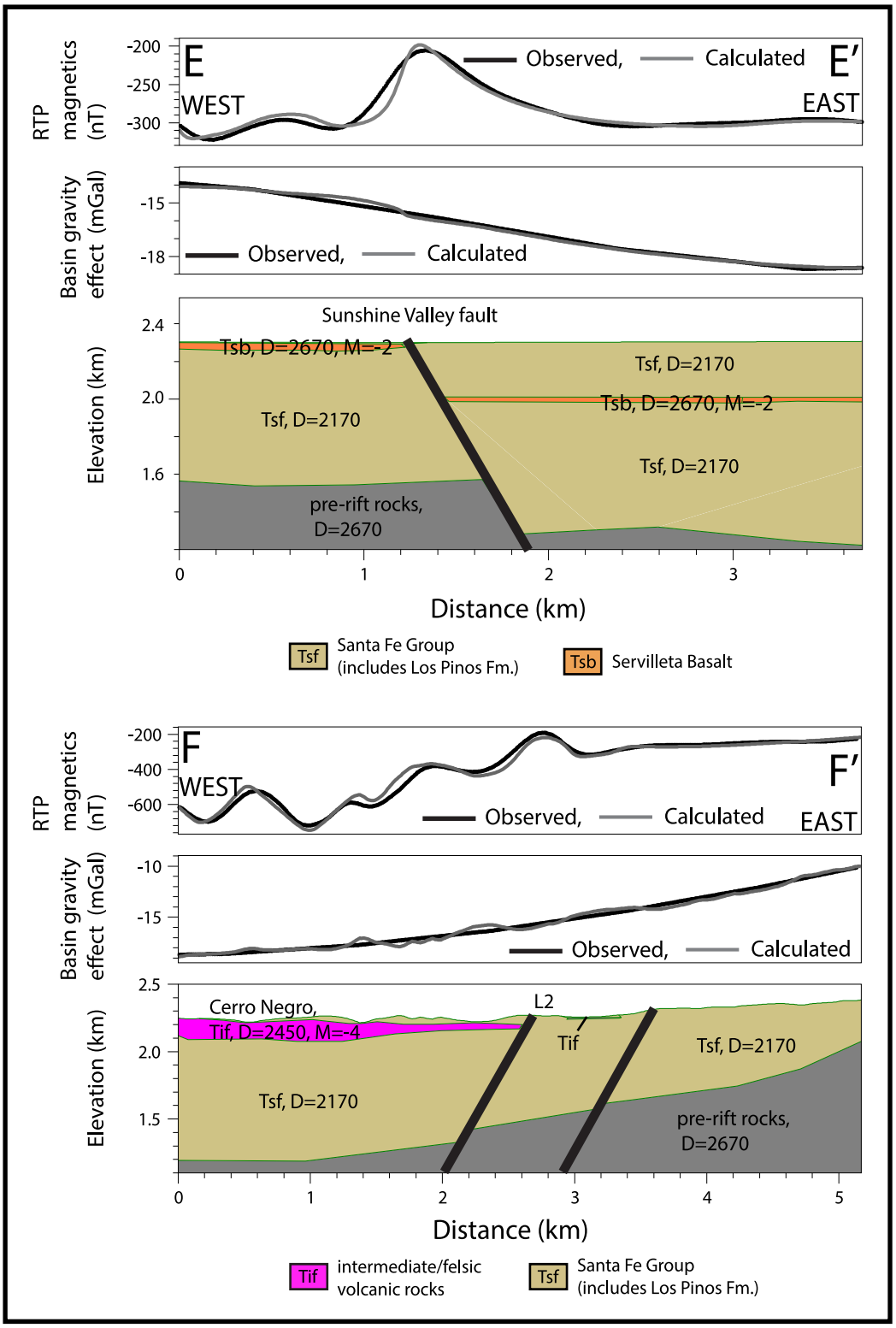


Figure 12. Magnetic and gravity profile models along E-E′ and F- F′. For each model, upper panel: reduced-to-pole (RTP) total-field aeromagnetic anomalies. For each model, middle panel: estimated gravitational effect of low-density basin fill ("Observed") and calculated model response. Magnetizations (M) in A/m (negative values indicate reversed magnetization); densities (D) in kg/m^3. No vertical exaggeration. Sunshine Valley fault and other interpreted normal faults shown.

Downloaded from https://pubs.geoscienceworld.org/uwyo/rmg/article-pdf/54/2/97/4907139/05402097.pdf
by USGS Library, Benjamin Drenth

margin, perhaps a hinge zone for an eastward-thickening half graben, or resulting from a structural displacement that is distributed over a broad fault zone (Fig. 7). The western part of the subbasin is covered by rocks of the Servilleta Basalt, indicating that major tectonic activity (i.e., enough to be resolvable in the gravity model) has not occurred along the western margin since the end of the Pliocene.

The Sunshine Valley fault has focused post-Pliocene subsidence in the eastern portion of the subbasin. The east-down Quaternary Sunshine Valley fault is known from water well data to offset the Servilleta Basalt within the subbasin (Fig. 7) (Winograd, 1959; Ruleman et al., 2013), forming a relatively narrow (~6 km) north-striking zone of maximum overall subsidence that resembles an elongate graben in map view (Figs. 6 and 11A–B). This is well expressed in aeromagnetic data that show an abrupt change in anomaly patterns at the Sunshine Valley fault (Fig. 11A). To the west, the busy pattern is consistent with the Servilleta Basalt lying at or near the surface. To the east, the smoother pattern indicates a much greater depth to magnetic rocks. Estimates of depth to magnetic anomaly sources (not shown) indicate ~400 m or more of east-down offset of the Servilleta Basalt by the Sunshine Valley fault. A simple magnetic model demonstrates that the aeromagnetic lineament associated with the Sunshine Valley fault can be explained by reversely magnetized Servilleta Basalt offset along an east-down fault, with a moderately magnetic basement of pre-rift rocks making a small contribution (E-E', Fig. 12).

Questa Subbasin

The Questa subbasin is imaged as a relatively small (~9-km diameter), subcircular-shaped structural low between the Rio Grande and southern Sangre de Cristo fault zone. It is estimated to have a maximum thickness of about 800 m of low-density basin fill, a result that both the 3D gravity model and MT modeling (Figs. 5, 6, and 8) independently support. This thickness estimate is much thinner than the ~3.5–4 km previously estimated (Keller et al., 1984), mainly a result of the 3D gravity modeling approach used here, which found low-density pre-rift rocks in the area of the subbasin. In other words, a significant portion of the gravity low over the subbasin is interpreted to be caused by the low-density pre-rift rocks, meaning that less of the gravity low is interpreted to be due to low-density basin fill.

The low-density rocks of the Latir volcanic locus, including the interpreted felsic batholith (Cordell et al., 1985), provide an explanation for the low-density pre-rift rocks in the 3D gravity model. Those rocks are here interpreted as extending under the subbasin (Fig. 5), consistent with the interpretation of Lipman and Reed (1989).

The subbasin overlaps geographically with the extent of Guadalupe Mountain (Figs. 4 and 8). Two-dimensional gravity modeling (Bauer et al., 2015; Grauch et al., 2015) and MT modeling (Fig. 8) each independently support the volcanic rocks of Guadalupe Mountain being underlain by a significant thickness (> 400 m) of low-density basin fill.

The Questa subbasin may be underlain by pre-rift and transitional Oligocene volcanic rocks (Bauer et al., 2015), similar to those that crop out nearby at Brushy Mountain (Thompson et al., 1986; Thompson et al., in press), in addition to the likelihood that rocks of the Latir volcanic locus and Questa caldera, such as the Amalia Tuff, are present at depth. It is possible that an unusually large amount of intracaldera Amalia Tuff is present in the subsurface, given that the western part of the caldera may underlie the subbasin (Lipman and Reed, 1989), and further that it may dominate the interpreted volume of low-density basin fill. Such a possibility cannot be ruled out from the 3D gravity modeling alone. However, MT modeling indicates that the portion of the caldera near the southern Sangre de Cristo fault zone and the Questa subbasin is characterized by relatively high resistivities (> 100 ohm-m), and that these resistivities extend westward under the subbasin in a pattern that matches the gravity-derived thickness estimate within ~200 m (Fig. 8). This pattern suggests that the low-density basin fill of the Questa subbasin, as here mainly defined by the 3D gravity modeling, is volumetrically dominated by deposits younger than the Amalia Tuff, the syn-rift Santa Fe Group.

The dominant subbasin-forming structure is the southern Sangre de Cristo fault zone at the eastern margin; the Gorge fault zone forms the western and northwestern margins of the Questa subbasin (Figs. 6, 8, and 11). A significant amount of subsidence occurred basinward of the present location of the southern Sangre de Cristo fault zone (Fig. 8) along west-down faults that lack Quaternary displacement (Fig. 3), a pattern consistent with eastward migration of the range front fault zone over time.

Boundary Between Sunshine Valley and Questa Subbasins

The Questa subbasin is separated from the Sunshine Valley subbasin by an interpreted structural high imaged as a narrow (~5 km wide) zone buried under less than 600 m of low-density basin fill (Figs. 6 and 11). An ~6-km eastward step of the Gorge fault zone forms the northwestern margin of the Questa subbasin and the western part of the structural high, corresponding in location with an eastward promontory of the Tres Piedras platform. Prominent aeromagnetic highs lie over this step and the southern edge of the intrabasin structural high, on the northeast margin of the aeromagnetic low produced by the northern part of Guadalupe Mountain (Fig. 11A–B). The source(s) of the aeromagnetic highs is (are) plausibly Proterozoic or pre-rift volcanic rocks that locally reach relatively shallow depths. Alternatives are transitional or rift-related volcanic rocks that form the basement to the low-density basin fill, or volcanic rocks related

Downloaded from https://pubs.geoscienceworld.org/uwyo/rmg/article-pdf/54/2/97/4907139/05402097.pdf
by USGS Library, Benjamin Drenth

to Guadalupe Mountain that may be underlain by a small thickness of low-density basin fill. The northern edge of the structural high is similar in location to the northern margin of the Questa caldera (Figs. 5 and 11). This similarity in location suggests a possible structural relationship between the two.

Boundary Between Taos and Questa Subbasins

The structural high that separates the Questa and Taos subbasins is coincident in location with the northeast-down Red River faults (Bauer et al., 2015; Thompson et al., in press). A concealed, intrabasin structural high is imaged extending from the Sangre de Cristo Mountains northwest to the Brushy-Timber Mountains' horst (Figs. 6 and 11). However, the structural high is wider than the area encompassed by the Red River faults, has much greater structural offset than that observed at the surface along the Red River faults (Bauer et al., 2015), and is likely to be controlled on its southern margin with the Taos subbasin by concealed southwest-down faults. The structural high must therefore be a broader and longer-lived feature than that implied solely by the extent of and sense of motion on the Red River faults. The southeastward projection of the structural high into the Sangre de Cristo Mountains is at a location where a range front promontory changes trend from northwest on the south side to north–northeast on the north side (Fig. 11B), forming a recognized boundary among different parts of the southern Sangre de Cristo fault zone (Ruleman and Machette, 2007). The fault zone on the south side of the promontory projects directly northwest into the structural high and Red River faults (Figs. 6 and 11B), suggestive of a continuous structural zone.

The structural high at the subbasin boundary is crossed by a northeast-striking fault indicated by aeromagnetic lineament L1, which divides a "busy" aeromagnetic pattern on the northwest from a smooth pattern of lower values to the southeast in an area mapped as surficial deposits (Fig. 11A). No Quaternary faults are associated with the L1 lineament. The different aeromagnetic patterns are consistent with shallow volcanic rocks to the northwest juxtaposed to the southeast against (1) a thick pile of weakly magnetized sediments (a southeast-down normal fault); or (2) weakly magnetic pre-rift rocks covered with sediments (northwest-down normal or strike-slip fault) (Fig. 11A–B). The southeast-down normal fault interpretation is not favored, because it is inconsistent with the local deepening direction of the Questa subbasin as indicated by the 3D gravity model, as well as detailed geophysical data and geologic cross sections near Guadalupe Mountain that indicate northwest-down subsidence (Bauer et al., 2015). A dominantly strike-slip fault that juxtaposes weakly magnetized pre-rift and volcanic rocks at depth may be the best interpretation, because the 3D gravity model indicates L1 marks the margins of both northwest-deepening (Questa) and southeast-deepening (Taos) subbasins and crosses the structural high (Fig. 11A–B). Weakly magnetized pre-rift rocks are likely to be crystalline basement rocks similar to the ones in the adjacent Sangre de Cristo Mountains.

The lack of strongly magnetized volcanic rocks southeast of lineament L1 suggests that either fault scarps blocked volcanic flows from traveling to the southeast or the volcanic rocks were eroded from the southeastern area after faulting. The latter explanation is preferred, due to the presumed difficulty in maintaining a topographically significant fault scarp formed on sediments. This implies that at least some slip occurred after those Pliocene volcanic rocks were emplaced.

Taos Subbasin

The Taos subbasin is imaged as a crudely D-shaped structure, with an estimated maximum 1.8-km thickness of low-density basin fill (Figs. 6 and 9; Grauch et al., 2017). This estimate is less than a previous estimate of > 3 km (Keller et al., 1984). The subbasin's southern and eastern margins contain the dominant structures that controlled rift-related subsidence, the Embudo and southern Sangre de Cristo fault zones, respectively. Gravity modeling indicates that the largest offsets on the subbasin-controlling faults are located basinward of the modern location of the southern Sangre de Cristo fault zone (Figs. 6 and 9). This is consistent with detailed modeling by Grauch et al. (2017), indicating that deformation along the fault zone increasingly shifted toward the current eastward location during latter stages of subbasin formation. The Gorge fault zone forms the northwestern margin, separating the Taos subbasin from the Brushy-Timber Mountains' horst. The boundary between the Taos and Tres Orejas subbasins is more diffuse (Figs. 6 and 9). This suggests that the Taos subbasin was superimposed on the southern part of the Tres Orejas subbasin, presumably as the Embudo fault zone developed.

Aeromagnetic lineament L2 along the northeast margin of Cerro Negro separates a "busy" pattern of aeromagnetic anomalies on the southwest from smoother anomalies to the northeast (Fig. 11A). This pattern is consistent with a southwest-down normal fault, where strongly reversely magnetized volcanic rocks of Cerro Negro on the southwest are juxtaposed against weakly magnetized sediments (also perhaps shallow, weakly magnetized crystalline rocks) to the northeast. The southwest-down sense of displacement and location of L2 generally parallels the northeastern margin of the Taos subbasin as indicated by the 3D gravity model (Fig. 11A–B). A simple gravity and magnetic model across Cerro Negro and the inferred L2 fault zone (F-F′ on Fig. 12) shows that ~900 m of Santa Fe Group sediments likely underlie Cerro Negro, similar to the conditions at Guadalupe Mountain in the Questa subbasin (Fig. 8).

Downloaded from https://pubs.geoscienceworld.org/uwyo/rmg/article-pdf/54/2/97/4907139/05402097.pdf
by USGS Library, Benjamin Drenth

The lack of strongly magnetized volcanic rocks northeast of the lineament suggests that either fault scarps blocked volcanic flows from traveling to the northeast or that the volcanic rocks were eroded from the northeastern area. As with L1, the latter explanation is preferred, and this is supported locally by a small volume of reversely magnetized rocks (erosional remnants of volcanic rocks that once extended northeast of L2?) interpreted from the aeromagnetic data to be preserved in the shallow subsurface between interpreted strands of the L2 fault zone (Fig. 12). These relations imply that at least some slip occurred after the Pliocene volcanic rocks were emplaced. No Quaternary faults are observed near L2 that have the same northwest strike, suggesting that the slip associated with L2 stopped by the end of the Pliocene.

DISCUSSION

Basin Geometry and Implications

The southern San Luis Basin is estimated to be considerably shallower (maximum depths of ~2 km) than previous models suggested (e.g., Keller et al., 1984), which is expected to be important to future groundwater studies of the basin-fill aquifers. The reduced thickness modeled here results from the 3D gravity modeling approach, which takes into account the estimated expression of pre-rift rocks and separates that from the effect of the rift basin. The most dramatic example of how this modeling approach alters estimates of basin thickness comes from the Questa subbasin, adjacent to the Latir volcanic locus and the large gravity low produced by its underlying batholith. Previous models that did not account for the effect of the gravity low overestimated the amplitude of the gravity low due to the low-density basin fill, resulting in local depth estimates of 4 km or more (Lipman and Mehnert, 1979; Keller et al., 1984). A 3D accounting of the gravitational effects of the Latir volcanic locus and its batholith yield a Questa subbasin depth estimate of only 800 m.

The geophysical modeling also shows that the southern San Luis Basin is strongly segmented into a series of narrow subbasins that have different spatiotemporal patterns of development. The complex pattern of the composite basin is made up of discrete subbasins as well as the shallow basin depths that have strong similarities to basin geometries interpreted for the central San Luis Basin (Drenth et al., 2013). These geometries contrast starkly with those interpreted for the northern San Luis, Española, and central Albuquerque basins, which are characterized as spatially large, asymmetric half grabens filled with as much as 3 to 6 km of low-density fill (Brister and Gries, 1994; Kluth and Schaftenaar, 1994; Grauch et al., 2009; Grauch and Connell, 2013). The diversity of basin geometries compared to the general continuity of the steep, high-relief rift flanks of the Sangre de Cristo Mountains along the eastern margins of the San Luis Basin southward to the Albuquerque Basin (Fig. 1) also challenges expected correlations between deep extensional basins and high-relief rift-flank uplifts (Vening-Meinesz, 1950; Wernicke and Axen, 1988). The variations in the basin depths within this stretch of the rift are not reflected in variations in the steepness nor relief of the rift-flank uplifts, suggesting further study on the timing and mechanisms of basin formation is required. For example, the relative shallowness of the Questa subbasin suggests that extensional strain was partly accommodated by processes other than basin subsidence. Could this be explained by rift extension in the Proterozoic rocks of the Sangre de Cristo Mountains, or magmatic dilation (e.g., diking) related to the assembly of the Taos Plateau volcanic field?

Although basins with large, deep half grabens are commonly used to represent typical basin geometry of the Rio Grande rift in the classic literature (e.g., Baldridge et al., 1995; Chapin and Cather, 1994), the shallow, complexly segmented geometries geophysically observed in the central and southern portions of the San Luis Basin demonstrate its greater tectonic diversity. Moreover, the shallow, complexly segmented geometries of the central and southern portions of the basin extend across about 100 km, a significant length that should be recognized as an important characteristic of basins of the Rio Grande rift.

Major Structures

Modeling presented here supports the conventional wisdom that the Embudo and southern Sangre de Cristo fault zones are the dominant structures that controlled the syn-rift (roughly post 20 Ma) development of the southern San Luis Basin. The greatest estimated thicknesses of low-density basin fill lie adjacent to these fault zones, indicating that they were the primary tectonic features active during Santa Fe Group deposition. These observations suggest that the low-density and conductive basin fill imaged by the gravity and MT modeling is volumetrically dominated by syn-rift—as opposed to transitional—sedimentary units.

Other significant syn-rift structures imaged here include the Gorge fault zone, an unnamed fault zone bounding the western margin of the Tres Orejas subbasin, and the structural highs that separate the Sunshine Valley, Questa, and Taos subbasins. Each of these structures is largely or entirely concealed from direct observation. The Gorge fault zone, as interpreted here, supports the general concepts published by previous workers in different parts of the southern San Luis Basin (Cordell, 1978; Lipman and Mehnert, 1979; Cordell and Keller, 1984; Dungan et al., 1984; Keller et al., 1984; Cordell et al., 1985; Bauer and Kelson, 2004; Grauch and Keller, 2004; Ruleman et al., 2013; Thompson et al., in press). Our results further support the model that the Gorge fault zone forms an abrupt structural boundary between the Sunshine Valley and Questa subbasins and Tres Piedras plat-

Downloaded from https://pubs.geoscienceworld.org/uwyo/rmg/article-pdf/54/2/97/4907139/05402097.pdf
by USGS Library, Benjamin Drenth

form to the west, covered with much thinner low-density basin fill (e.g., Lipman and Mehnert, 1979).

The observations of geophysical character and interpretations of the Gorge fault zone presented here are speculatively consistent with a long-lived, reactivated structural zone that may be significant to basin formation beyond the scale of the southern San Luis Basin. The interpreted trend of the Gorge fault zone is subparallel to another set of structures across the state line in Colorado that control the western margin of the Costilla Plains structural depression and have been interpreted to have both pre-rift and syn-rift displacement (Drenth et al., 2013). Farther to the north, this northward-striking structural zone continues through the northern San Luis Basin along the eastern margin of the Alamosa horst (Gaca and Karig, 1965; Keller et al., 1984; Gries and Brister, 1989; Brister, 1990; Brister and Gries, 1994; Kluth and Schaftenaar, 1994). The Gorge fault zone as interpreted in the southern San Luis Basin may thus be part of a more geographically extensive series of generally north-striking structures that played a major role in basin formation, and speculatively may have pre-rift inheritance (i.e., the Picuris-Pecos fault zone?).

Evolution of the Southern San Luis Basin

Results of the 3D gravity modeling and insights from MT and aeromagnetic data allow development of a revised tectonic history of the southern San Luis Basin, although much of this revised history is speculative, because of the extensive cover. Nevertheless, this synthesis relies on a comparison of patterns of basin thickness expressed in the 3D gravity modeling to bedrock geology, combined with concepts of temporal and paleogeographic evolution developed by previous workers (Kelley and Duncan, 1986; Bauer and Kelson, 2004; Smith, 2004; Grauch et al., 2017; Turner et al., in press). The main elements of the synthesis developed here are summarized in Figure 13.

The transitional period between waning SRMVF magmatism and the onset of the main phase of Rio Grande rift tectonism, roughly 28–20 Ma (mainly Oligocene), involved eruptions of the uppermost tuffs from the southeastern San Juan Mountains, activity in the Latir volcanic locus, and erosion of the volcanic loci. Rocks of the San Juan Mountains' volcanic locus are preserved in the northern Tusas Mountains and thin abruptly to the southeast, suggesting that a structural high may have limited their southward and southeastward extent (Smith, 2004). The structural high imaged in the 3D gravity model extending from the Tusas Mountains eastward to the Tres Piedras platform (Fig. 6) may reflect this structural high. In the Latir volcanic locus, the Questa caldera formed at ~25 Ma and the subvolcanic batholith was emplaced. Rocks of the Latir volcanic locus extend westward to the Brushy and Timber mountains and across the basin to the same structural high, suggesting that much of what is now the Tres Piedras platform was covered with volcanic rocks erupted from the Latir volcanic locus. The Los Pinos Formation and lower members of the Picuris Formation record erosion of the volcanic loci and deposition into thin structural lows, such as the Las Mesitas graben. Similar deposits almost certainly blanketed the whole region that is now the southern San Luis Basin, and structural lows similar in form to the Las Mesitas graben may be preserved today near the base of the various subbasins imaged in the 3D gravity model. Basaltic lavas of the Hinsdale Formation were erupted across the broader area of the Las Mesitas graben. The Picuris-Pecos fault zone was active (with waning activity) at this time, as indicated by the preservation of Picuris Formation rocks within the fault zone south and east of the Embudo fault zone (Fig. 3). The northward extent of the Picuris-Pecos fault zone slip during this time period is unknown.

The 3D gravity model is dominated by tectonic elements of the southern San Luis Basin that developed during the Miocene, after ~20 Ma (e.g., Kelley and Duncan, 1986) and prior to the development of the ~5.2–2.9 Ma Taos Plateau volcanic field. Rio Grande rift tectonism and subsidence were marked by the rise of the Sangre de Cristo Mountains, corresponding formation of the southern Sangre de Cristo fault zone at the eastern margin of the basin, and the formation of the Embudo fault zone. The development of the Tres Orejas subbasin, or at least the main portion of the subbasin imaged in the 3D gravity model, was controlled by transtensional, sinistral north-down slip on the Embudo fault zone at its southern margin and by east-down slip on a now-concealed normal fault zone at its western margin. This structure was also partly responsible for forming the structural high at the southwestern basin margin associated with Cerro Azul. The Sunshine Valley, Questa, and Taos subbasins and their intervening structural highs formed during this time, controlled mainly by the west-down southern Sangre de Cristo fault zone along their eastern margins, and to a lesser extent by the east-down Gorge fault zone and perhaps hinge zones(?) along their western margins. The western portion of the Questa caldera was cut by the southern Sangre de Cristo fault zone and dropped to the west where it floors the Questa subbasin. The Tres Piedras platform emerged as a broad structural high, and little or no deposition occurred there. The relationship between the Tres Orejas and Taos subbasins is less clear. Displacement on the Gorge fault zone, the boundary between the two, decreases southward such that it is difficult to precisely locate that boundary in the vicinity of the Embudo fault zone. It appears likely that the Taos subbasin is superimposed on part of the Tres Orejas subbasin.

Following the development of the Taos Plateau volcanic field, rift-related subsidence became more tightly focused on the eastern and southeastern basin margins, controlled by the southern Sangre de Cristo fault zone and Embudo fault

Downloaded from https://pubs.geoscienceworld.org/uwyo/rmg/article-pdf/54/2/97/4907139/05402097.pdf
by USGS Library, Benjamin Drenth

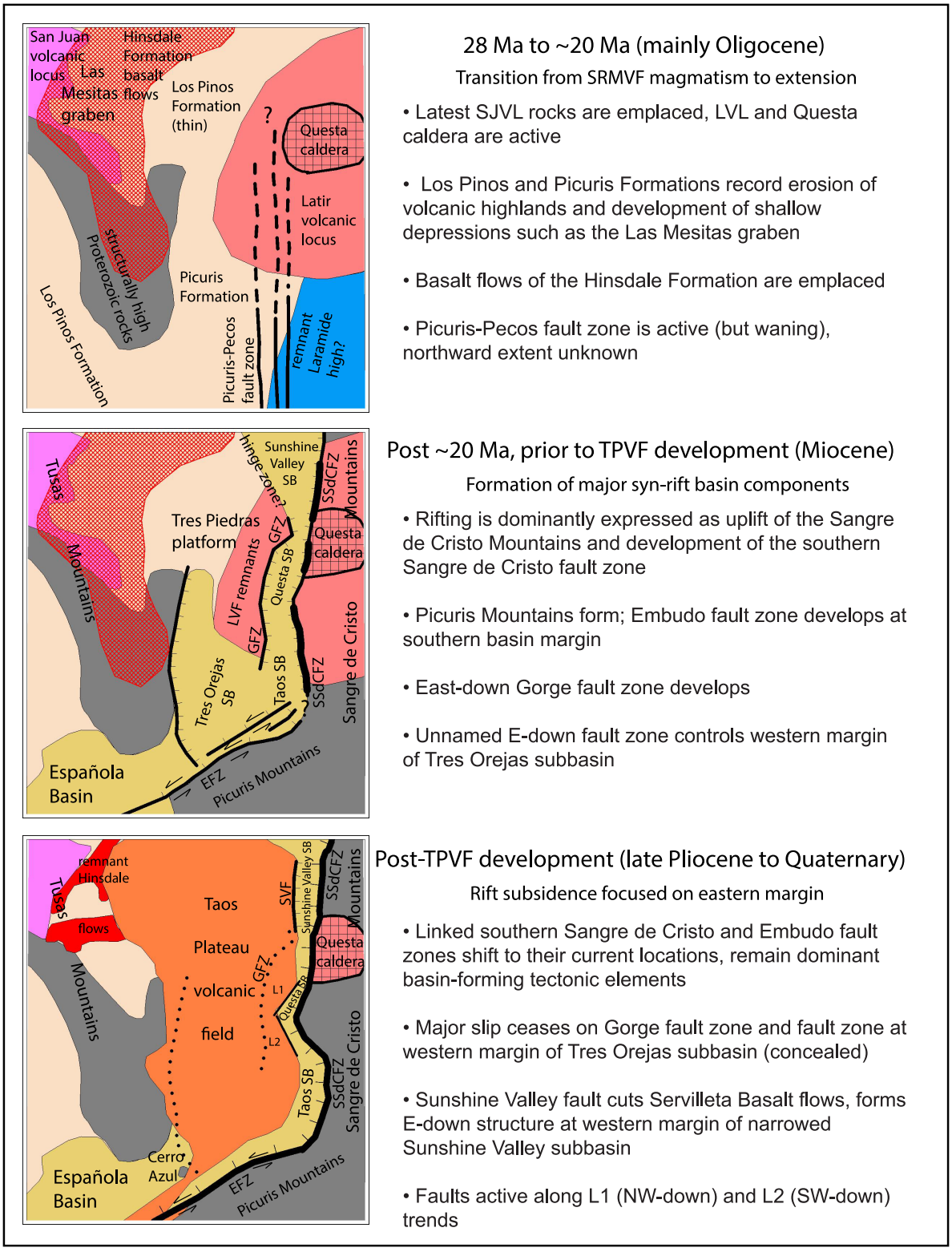


Figure 13. Schematic conceptual evolution of the southern San Luis Basin, focused on major basin- and subbasin-forming structures and events addressed by this study. SRMVF: Southern Rocky Mountain volcanic field. SJVL: San Juan volcanic locus. LVL: Latir volcanic locus. TPVF: Taos Plateau volcanic field. SSdCFZ: southern Sangre de Cristo fault zone. EFZ: Embudo fault zone. GFZ: Gorge fault zone. SB: subbasin.

Downloaded from https://pubs.geoscienceworld.org/uwyo/rmg/article-pdf/54/2/97/4907139/05402097.pdf
by USGS Library, Benjamin Drenth

zone. Significant portions of those dominant basin-forming structures, especially those south of the latitude of the Questa caldera, shifted location toward the Sangre de Cristo and Picuris mountains' fronts. A lack of significant displacements recognized in the field indicates that major slip on the Gorge fault zone and the fault zone at the western margin of the Tres Orejas subbasin had ceased by this time. Subsidence of and deposition within the Tres Orejas subbasin had also stopped, except for perhaps a narrow zone at its southern margin with the Embudo fault zone. The actively subsiding portion of the Sunshine Valley subbasin narrowed considerably, with the east-down Sunshine Valley fault developing antithetic to the southern Sangre de Cristo fault zone and forming the western margin of the deforming part of the subbasin. The Sunshine Valley fault probably formed as a northern extension of the Gorge fault zone. The structural highs separating the Sunshine Valley, Questa, and Taos subbasins likely continued to be active during this time. The northwest-striking Red River faults lie along the southern of the two structural highs, subparallel in strike to the Sangre de Cristo Mountains front and the L2 fault(s). This strike is cut by L1 fault(s), suggesting a complex history of development for the structural high.

CONCLUSIONS

3D gravity modeling, coupled with information from MT data, aeromagnetic data, and geologic mapping, yields new perspectives on the geometry, thickness, and spatiotemporal evolution of the southern San Luis Basin of the Rio Grande rift. The basin is shown to be both shallower and more segmented in the subsurface, with narrower zones of rift-related subsidence, than indicated or implied by previous models. Estimated thicknesses of low-density basin fill are at most ~2 km, and much of the basin is significantly shallower. These results are expected to be significant to future groundwater modeling efforts.

The southern San Luis Basin records the transition from SRMVF magmatism to basin subsidence and volcanism related to the Rio Grande rift. Evidence of mainly Oligocene deposition of the Los Pinos Formation is preserved in the narrow (~400 m) Las Mesitas graben in the northeastern Tusas Mountains. The dominant tectonic features related to rifting initially formed in Miocene time along the eastern and southeastern basin margins, including the Embudo and southern Sangre de Cristo fault zones. The Sunshine Valley, Questa, Taos, and Tres Orejas subbasins formed with those fault zones controlling their eastern and southeastern margins. The east-down Gorge fault zone controlled the western margin of the Sunshine Valley, Questa, and Taos subbasins; the western margin of the Tres Orejas subbasin was controlled by a hypothesized east-down fault zone. Major tectonic activity along the Gorge fault zone and within the Tres Orejas subbasin ceased by the end of the development of the largely Pliocene Taos Plateau volcanic field. Rift-related subsidence became more narrowly focused on the eastern margin of the basin. The linked southern Sangre de Cristo and Embudo fault zones continued to be the dominant structures controlling basin development, with the Sunshine Valley, L1, and L2 faults playing important secondary roles controlling subsidence internal to the basin.

ACKNOWLEDGMENTS

This work was supported by the National Cooperative Geologic Mapping and Mineral Resource Programs of the U.S. Geological Survey. Taos Pueblo, through the facilitation of Gil Suazo, generously granted access to collect gravity data that significantly improved the quality of the model presented here. Bryanna Sudman, Michael Wussow, Lauren Howell, Dr. Stan Love, and Taos Regional Airport staff assisted with or facilitated various aspects of gravity data collection. Carson National Forest staff, especially John Grasso, provided helpful assistance during gravity data collection in the Tusas Mountains. Peggy Johnson provided important borehole information. Adam Read assisted with compilation of geologic data. Michael Machette, Phil Wannamaker, Paul Bedrosian, and Tony Benson provided helpful insights at various stages of this work. We thank Arthur Snoke, Ronald Frost, Diane Doser, Mark Hudson, Randy Keller, and Julie Herrick for helpful reviews that significantly improved this paper. Robert Waggener and Brendon Orr provided helpful editorial support.

REFERENCES CITED

Aby, S., 2008, Geologic map of the Servilleta Plaza quadrangle, Taos County, New Mexico: New Mexico Bureau of Geology and Mineral Resources Open-File Geologic Map 182, scale 1:24,000, 1 sheet, 12 p. text.

Aby, S.B., Bauer, P.W., and Kelson, K.I., 2004, The Picuris Formation: A late Eocene to Miocene sedimentary sequence in northern New Mexico, *in* Brister, B.S., Bauer, P.W., Read, A.S., and Lueth, V.W., eds., Geology of the Taos Region: New Mexico Geological Society, 55th Fall Field Conference, Guidebook, p. 335–350.

Aby, S., Karlstrom, K., Koning, D., and two others, 2010, Geologic map of the Las Tablas quadrangle, Rio Arriba County, New Mexico: New Mexico Bureau of Geology and Mineral Resources Open-File Geologic Map 200, 1:24,000 scale, 1 sheet, 30 p. text.

Ailes, C.E., and Rodriguez, B.D., 2010, Magnetotelluric data, Taos Plateau volcanic field, New Mexico: U.S. Geological Survey Open-File Report 2010-1245, *iv* + 65 p.

___2015, Magnetotelluric data collected to characterize aquifers in the San Luis Basin, New Mexico: U.S. Geological Survey Open-File Report 2014-1248, *iv* + 9 p., http://dx.doi.org/10.3133/ofr20141248.

Downloaded from https://pubs.geoscienceworld.org/uwyo/rmg/article-pdf/54/2/97/4907139/05402097.pdf
by USGS Library, Benjamin Drenth

Anderson, O.J., and Jones, G.E., 1994, Geologic map of New Mexico: New Mexico Bureau of Mines and Mineral Resources Open-File Report 408-A and B, geologic map and 15 magnetic disks, 1:500,000 scale, 2 sheets, 59 p. text.

Appelt, R.M., 1998, $^{40}Ar/^{39}Ar$ geochronology and volcanic evolution of the Taos Plateau volcanic field, northern New Mexico and southern Colorado [Master's thesis]: Socorro, New Mexico, New Mexico Institute of Mining and Technology, 58 p.

Baldridge, W.S., Keller, G.R., Haak, V., and three others, 1995, The Rio Grande rift, *in* Olsen, K.H., ed., Continental rifts: Evolution, structure, and tectonics (first edition, v. 25): Amsterdam, The Netherlands, Elsevier, p. 233–275.

Baltz, E.H., 1978, Résumé of the Rio Grande depression in north-central New Mexico, *in* Hawley, J.W., ed., Guidebook to Rio Grande rift in New Mexico and Colorado: New Mexico Bureau of Mines and Mineral Resources, Circular 163, p. 210–228.

Baltz, E.H., and Myers, D.A., 1999, Stratigraphic framework of upper Paleozoic rocks, southeastern Sangre de Cristo Mountains, New Mexico, with a section on speculations and implications for regional interpretation of Ancestral Rocky Mountains paleotectonics: New Mexico Bureau of Mines and Mineral Resources Memoir 48, 272 p.

Bankey, V., Grauch, V.J.S., and Fugro Airborne Surveys Corp., 2004, Digital aeromagnetic data and derivative products from a helicopter survey over the town of Taos and surrounding areas, Taos County, New Mexico: U.S. Geological Survey Open-File Report 2004-1229-A, 7 p., https://pubs.usgs.gov/of/2004/1229/A/.

Bankey, V., Grauch, V.J.S., Drenth, B.J., and Geophex Ltd., 2006, Digital data from the Questa-San Luis and Santa Fe East helicopter magnetic surveys in Santa Fe and Taos counties, New Mexico, and Costilla County, Colorado: U.S. Geological Survey Open-File Report 2006-1170, *ii* + 6 p., https://pubs.usgs.gov/of/2006/1170/.

Bankey, V., Grauch, V.J.S., Webbers, A., and PRJ Inc., 2005, Digital data and derivative products from a high-resolution aeromagnetic survey of the central San Luis Basin, covering parts of Alamosa, Conejos, Costilla, and Rio Grande counties, Colorado, and Taos County, New Mexico: U.S. Geological Survey Open-File Report 2005-1200, *ii* + 9 p., https://pubs.usgs.gov/of/2005/1200/.

Baranov, V., and Naudy, H., 1964, Numerical calculation of the formula of reduction to the magnetic pole: Geophysics, v. 29, p. 67–79.

Barker, F., 1958, Precambrian and Tertiary geology of the Las Tablas quadrangle, New Mexico: New Mexico Bureau of Mines and Mineral Resources Bulletin 45, *vi* + 104 p.

Bauer, P.W., 1993, Proterozoic tectonic evolution of the Picuris Mountains, northern New Mexico: The Journal of Geology, v. 101, p. 483–500.

Bauer, P.W., and Kelson, K. ., 1997, Geologic map of the Taos SW 7.5-minute quadrangle, Taos County, New Mexico: New Mexico Bureau of Mines and Mineral Resources Open-File Geologic Map 12, scale 1:24,000, 1 sheet, 5 p. text.

___2004, Cenozoic structural development of the Taos area, New Mexico, *in* Brister, B.S., Bauer, P.W., Read, A.S., and Lueth, V.W., eds., Geology of the Taos Region: New Mexico Geological Society, 55th Fall Field Conference, Guidebook, p. 129–146.

Bauer, P.W., and Ralser, S., 1995, The Picuris-Pecos fault—Repeatedly reactivated, from Proterozoic(?) to Neogene, *in* Bauer, P.W., Kues, B.S., Dunbar, N.W., and two others, eds., Geology of the Santa Fe Region: New Mexico Geological Society, 46th Fall Field Conference, Guidebook, p. 111–115.

Bauer, P.W., and Williams, M.L., 1989, Stratigraphic nomenclature of Proterozoic rocks, northern New Mexico—revisions, redefinitions, and formalization: New Mexico Geology, v. 11, p. 45–52.

Bauer, P.W., Grauch, V.J.S., Johnson, P.S., and three others, 2015, Geologic cross sections and preliminary geologic map of the Questa area, Taos County, New Mexico: New Mexico Bureau of Geology and Mineral Resources Open-File Report 578, scale 1:24,000, 2 sheets, 16 p. text.

Bauer, P.W., Kelson, K.I., Aby, S.B., and three others, 2000, Geologic map of the Ranchos de Taos 7.5-minute quadrangle, Taos County, New Mexico: New Mexico Bureau of Mines and Mineral Resources Open-File Geologic Map 33, scale 1:24,000, 1 sheet, 3 p. text.

Bauer, P.W., Kelson, K.I., Grauch, V.J.S., and four others, 2016, Geologic map and cross sections of the Embudo fault zone in the southern Taos Valley, Taos County, New Mexico: New Mexico Bureau of Geology and Mineral Resources Open-File Report 584, scale 1:24,000, 2 sheets, 28 p. text.

Blakely, R.J., 1995, Potential theory in gravity & magnetic applications: Cambridge, United Kingdom, Cambridge University Press, *xix* + 441 p.

Blakely, R.J., and Jachens, R.W., 1991, Regional study of mineral resources in Nevada—Insights from three-dimensional analysis of gravity and magnetic anomalies: Geological Society of America Bulletin, v. 103, p. 795–803.

Brister, B.S., 1990, Tertiary sedimentation and tectonics: San Juan sag-San Luis Basin region, Colorado and New Mexico [Ph.D. dissert.]: Socorro, New Mexico, New Mexico Institute of Mining and Technology, 267 p.

Brister, B.S., and Gries, R.R., 1994, Tertiary stratigraphy and tectonic development of the Alamosa Basin (northern San Luis Basin), Rio Grande rift, south-central Colorado, *in* Keller, G.R., and Cather, S.M., eds., Basins of the Rio Grande rift: Structure, stratigraphy, and tectonic setting: Boulder, Colorado, Geological Society of America Special Paper 291, p. 39–58.

Downloaded from https://pubs.geoscienceworld.org/uwyo/rmg/article-pdf/54/2/97/4907139/05402097.pdf
by USGS Library, Benjamin Drenth

Brown, L.L., Caffall, N.M., and Golombek, M.P., 1993, Paleomagnetism and tectonic interpretations of the Taos Plateau volcanic field, Rio Grande rift, New Mexico: Journal of Geophysical Research, v. 98, no. B12, p. 22,401–22,413.

Butler, A.P., Jr., 1946, Tertiary and Quaternary geology of the Tusas-Tres Piedras area, New Mexico [Ph.D. dissert.]: Cambridge, Massachusetts, Harvard University, 188 p.

___1971, Tertiary volcanic stratigraphy of the eastern Tusas Mountains, southwest of the San Luis Valley, Colorado-New Mexico, *in* James, H.L., ed., San Luis Basin: New Mexico Geological Society, 22nd Fall Field Conference, Guidebook, p. 289–300.

Cather, S.M., 2004, Laramide orogeny in central and northern New Mexico and southern Colorado, *in* Mack, G.H., and Giles, K.A., eds., The geology of New Mexico: A geologic history: New Mexico Geological Society, Special Publication 11, p. 203–248.

Cather, S.M., Karlstrom, K.E., Timmons, J.M., and Heizler, M.T., 2006, Palinspastic reconstruction of Proterozoic basement-related aeromagnetic features in north-central New Mexico: Implications for Mesoproterozoic to late Cenozoic tectonism: Geosphere, v. 2, p. 299–323.

Cather, S.M., Read, A.S., Dunbar, N.W., and four others, 2011, Provenance evidence for major post-Early Pennsylvanian dextral slip on the Picuris-Pecos fault, northern New Mexico: Geosphere, v. 7, p. 1,175–1,193.

Chapin, C.E., and Cather, S.M., 1994, Tectonic setting of the axial basins of the northern and central Rio Grande rift, *in* Keller, G.R., and Cather, S.M., eds., Basins of the Rio Grande rift: Structure, stratigraphy, and tectonic setting: Boulder, Colorado, Geological Society of America Special Paper 291, p. 5–25.

Clark, D.A., 1997, Magnetic petrophysics and magnetic petrology: Aids to geological interpretation of magnetic surveys: AGSO Journal of Australian Geology & Geophysics, v. 17(2), p. 83–103.

Cordell, L., 1978, Regional geophysical setting of the Rio Grande rift: Geological Society of America Bulletin, v. 89, p. 1,073–1,090.

___1979, Gravimetric expression of graben faulting in Santa Fe country and the Espanola Basin, New Mexico, *in* Ingersoll, R.V., Woodward, L.A., and James, H.L., eds., Santa Fe Country: New Mexico Geological Society, 30th Fall Field Conference, Guidebook, p. 59–64.

Cordell, L., and Grauch, V.J.S., 1985, Mapping basement magnetization zones from aeromagnetic data in the San Juan Basin, New Mexico, *in* Hinze, W.J., ed., The utility of regional gravity and magnetic anomaly maps: Tulsa, Oklahoma, Society of Exploration Geophysicists, p. 181–197.

Cordell, L., and Keller, G.R., 1984, Regional structural trends inferred from gravity and aeromagnetic data in the New Mexico-Colorado border region: *in* Baldridge, W.S., Dickerson, P.W., Riecker, R.E., and Zidek, J., eds., Rio Grande rift: Northern New Mexico: New Mexico Geological Society, 35th Fall Field Conference, Guidebook, p. 21–23.

Cordell, L., Long, C.L., and Jones, D.W., 1985, Geophysical expression of the batholith beneath Questa caldera, New Mexico: Journal of Geophysical Research, v. 90, no. B13, p. 11,263–11,269.

Cosca, M.A., Thompson, R.A., and Turner, K.J., 2014, High precision $^{40}Ar/^{39}Ar$ geochronology of Servilleta Basalts of the Rio Grande Gorge, New Mexico: American Geophysical Union, 2014 Fall Meeting, San Francisco, California, Abstract V51A–4728.

Daniel, C.G., Karlstrom, K.E., Williams, M.L., and Pedrick, J.N., 1995, The reconstruction of a middle Proterozoic orogenic belt in north-central New Mexico, USA, *in* Bauer, P.W., Kues, B.S., Dunbar, N.W., and two others, eds., Geology of the Santa Fe Region: New Mexico Geological Society, 46th Fall Field Conference, Guidebook, p. 193–200.

Deszcz-Pan, M., Rodriguez, B.D., Doucette, J.P., and six others, 2000, Digital airborne time domain electromagnetic data from surveys over Cochiti Pueblo, Rio Puerco and Rio Rancho, New Mexico: U.S. Geological Survey Open-File Report 502, 13 p.

Drenth, B.J., 2016, Principal facts of gravity data in the southern San Luis Basin, northern New Mexico: U.S. Geological Survey data release, http://dx.doi.org/10.5066/F7JQ0Z5N.

Drenth, B.J., Grauch, V.J.S., and Rodriguez, B.D., 2013, Geophysical constraints on Rio Grande rift structure in the central San Luis Basin, Colorado and New Mexico, *in* Hudson, M.R., and Grauch, V.J.S., eds., New Perspectives on Rio Grande Rift Basins: From Tectonics to Groundwater: Boulder, Colorado, Geological Society of America Special Paper 494, p. 75–99.

Drenth, B.J., Keller, G.R., and Thompson, R.A., 2012, Geophysical study of the San Juan Mountains batholith complex, southwestern Colorado: Geosphere, v. 8, p. 669–684, https://doi.org/10.1130/GES00723.1.

Drenth, B.J., Turner, K.J., Thompson, R.A., and three others, 2011, Geophysical expression of elements of the Rio Grande rift in the northeast Tusas Mountains—Preliminary interpretations, *in* Koning, D.J., Karlstrom, K.E., Kelley, S.A., and two others, eds., Geology of the Tusas Mountains and Ojo Caliente: New Mexico Geological Society, 62nd Fall Field Conference, Guidebook, p. 165–175.

Dungan, M.A., Muehlberger, W.R., Leininger, L., and four others, 1984, Volcanic and sedimentary stratigraphy of the Rio Grande Gorge and the late Cenozoic geologic evolution of the southeastern San Luis Valley, *in* Baldridge, W.S., Dickerson, P.W., Riecker, R.E., and Zidek, J., eds., Rio Grande rift, northern New Mexico:

Downloaded from https://pubs.geoscienceworld.org/uwyo/rmg/article-pdf/54/2/97/4907139/05402097.pdf
by USGS Library, Benjamin Drenth

New Mexico Geological Society, 35th Fall Field Conference, Guidebook, p. 51–57.

Dungan, M.A., Thompson, R.A., and Stormer, J.S., 1989, Rio Grande rift volcanism: Northeastern Jemez zone, New Mexico, *in* Chapin, C.E., and Zidek, J., eds., Field excursions to volcanic terranes in the western United States, volume 1: Southern Rocky Mountain region: New Mexico Bureau of Mines and Mineral Resources Memoir 46, p. 435–486.

Gaca, J.R., and Karig, D.E., 1965, Gravity survey in the San Luis Valley area, Colorado: U.S. Geological Survey Open-File Report 66-46, *iii* + 48 p.

Grauch, V.J.S., and Connell, S.D., 2013, New perspectives on the geometry of the Albuquerque Basin, Rio Grande rift, New Mexico: Insights from geophysical models of rift-fill thickness, *in* Hudson, M.R., and Grauch, V.J.S., eds., New Perspectives on Rio Grande Rift Basins: From Tectonics to Groundwater: Boulder, Colorado, Geological Society of America Special Paper 494, p. 427–462.

Grauch, V.J.S., and Drenth, B.J., 2016, Physical properties by geologic unit in the southern San Luis Basin, New Mexico: U.S. Geological Survey data release, https://doi.org/10.5066/F7RJ4GMB.

Grauch, V.J.S., and Keller, G.R., 2004, Gravity and aeromagnetic expression of tectonic and volcanic elements of the southern San Luis Basin, New Mexico and Colorado, *in* Brister, B.S., Bauer, P.W., Read, A.S., and Lueth, V.W., eds., Geology of the Taos Region: New Mexico Geological Society, 55th Fall Field Conference, Guidebook, p. 230–243.

Grauch, V.J.S., Bauer, P.W., Drenth, B.J., and Kelson, K I., 2017, A shifting rift—Geophysical insights into the evolution of Rio Grande rift margins and Embudo transfer zone near Taos, New Mexico: Geosphere, v. 13, p. 870–910.

Grauch, V.J.S., Bauer, P.W., and Kelson, K.I., 2004, Preliminary interpretation of high-resolution aeromagnetic data collected near Taos, New Mexico, *in* Brister, B.., Bauer, P.W., Read, A.S., and Lueth, V.W., eds., Geology of the Taos Region: New Mexico Geological Society, 55th Fall Field Conference, Guidebook, p. 244–256.

Grauch, V.J.S., Drenth, B.J., Thompson, R.A., and Bauer, P.W., 2015, Preliminary geophysical interpretations of regional subsurface geology near the Questa mine tailing facility and Guadalupe Mountain, Taos County, New Mexico: U.S. Geological Survey Open-File Report 2015-1129, *vi* + 25 p.

Grauch, V.J.S., Phillips, J.D., Koning, D.J., and two others, 2009, Geophysical interpretations of the southern Española Basin, New Mexico, that contribute to understanding its hydrogeologic framework: U.S. Geological Survey Professional Paper 1761, *vi* + 88 p.

Green, G.N., and Jones, G.E., 1997, The digital geologic map of New Mexico in ARC/INFO format: U.S. Geological Survey Open-File Report 97-52, 9 p.

Gries, R.R., and Brister, B.S., 1989, New interpretation of seismic lines in the San Luis Valley, south-central Colorado, *in* Harmon, E.J., ed., Water in the valley: Colorado Groundwater Association, 8th Annual Field Trip, Guidebook, p. 241–254.

Hallenburg, J.K., 1998, Non-hydrocarbon methods of geophysical formation evaluation: Boca Raton, Florida, Lewis Publishers, 265 p.

Hearst, J.R., and Nelson, P.H., 1985, Well logging for physical properties: New York, New York, McGraw-Hill Book Co., 571 p.

Hearst, J.R., Nelson, P.H., and Paillet, F.L., 2000, Well logging for physical properties: A handbook for geophysicists, geologists and engineers (second edition): New York, New York, John Wiley & Sons, *ix* + 483 p.

Heywood, C.E., 1992, Isostatic residual gravity anomalies of New Mexico, U.S.: Geological Survey Water-Resources Investigations Report 91-4065, *iv* + 27 p.

Hinze, W.J., 2003, Bouguer reduction density, why 2.67?: Geophysics, v. 68, p. 1,559–1,560.

Hinze, W.J., von Frese, R.R.B., and Saad, A.H., 2013, Gravity and magnetic exploration: Principles, practices, and applications: New York, New York, Cambridge University Press, *xiv* + 512 p.

Hudson, M.R., and Grauch, V.J.S., 2013, Introduction, *in* Hudson, M.R., and Grauch, V.J.S., eds., New Perspectives on Rio Grande Rift Basins: From Tectonics to Groundwater: Boulder, Colorado, Geological Society of America Special Paper 494, p. v–xii.

Ingersoll, R.V., 2001, Structural and stratigraphic evolution of the Rio Grande rift, northern New Mexico and southern Colorado: International Geology Review, v. 43, p. 867–891.

Ingersoll, R.V., and Cavazza, W., 1991, Reconstruction of Oligo–Miocene volcaniclastic dispersal patterns in north-central New Mexico using sandstone petrofacies, *in* Fisher, R.V., and Smith, G.A., eds., Sedimentation in volcanic settings: SEPM (Society of for Sedimentary Geology), Special Publication 45, p. 227–236.

Ingersoll, R.V., Cavazza, W., Baldridge, W.S., and Shafiqullah, M., 1990, Cenozoic sedimentation and paleotectonics of north-central New Mexico: Implications for initiation and evolution of the Rio Grande rift: Geological Society of America Bulletin, v. 102, p. 1,280–1,296.

Jachens, R.W., and Moring, B.C., 1990, Maps of the thickness of Cenozoic deposits and the isostatic residual gravity over basement for Nevada: U.S. Geological Survey Open-File Report 90-404, 15 p.

Johnson, P.S., and Bauer, P.W., 2012, Hydrogeologic investigation of the northern Taos Plateau, Taos County, New Mexico: New Mexico Bureau of Geology and Mineral Resources Open-File Report 544, *viii* + 78 p. and four appendices.

Downloaded from https://pubs.geoscienceworld.org/uwyo/rmg/article-pdf/54/2/97/4907139/05402097.pdf
by USGS Library, Benjamin Drenth

Jones, J.V., III, Connelly, J.N., Karlstrom, K.E., and two others, 2009, Age, provenance, and tectonic setting of Paleoproterozoic quartzite successions in the southwestern United States: Geological Society of America Bulletin, v. 121, p. 247–264.

Jones, J.V., III, Daniel, C.G., Frei, D., and Thrane, K., 2011, Revised regional correlations and tectonic implications of Paleoproterozoic and Mesoproterozoic metasedimentary rocks in northern New Mexico, USA: New findings from detrital zircon studies of the Hondo Group, Vadito Group, and Marqueñas Formation: Geosphere, v. 7, p. 974–991.

Karlstrom, K.E., and Daniel, C.G., 1993, Restoration of Laramide right-lateral strike slip in northern New Mexico by using Proterozoic piercing points: Tectonic implications from the Proterozoic to the Cenozoic: Geology, v. 21, p. 1,139–1,142.

Keller, G.R., Cordell, L., Davis, G.H., and two others, 1984, A geophysical study of the San Luis Basin, *in* Baldridge, W.S., Dickerson, P.W., Riecker, R.E., and Zidek, J., eds., Rio Grande rift: Northern New Mexico: New Mexico Geological Society, 35th Fall Field Conference, Guidebook, p. 51–57.

Keller, G.V., 1987, Rock and mineral properties, *in* Nabighian, M.N., ed., Electromagnetic methods in applied geophysics, v. 1, Theory: Tulsa, Oklahoma, Society of Exploration Geophysicists, p. 13–51.

Keller, G.V., and Frischknecht, F.C., 1966, Electrical methods in geophysical prospecting: Oxford, United Kingdom, Pergamon Press, 517 p.

Kelley, S.A., and Duncan, I.J., 1986, Late Cretaceous to middle Tertiary tectonic history of the northern Rio Grande rift, New Mexico: Journal of Geophysical Research, v. 91, no. B6, p. 6,246–6,262.

Kelley, V.C., 1978, Geology of the Española Basin, New Mexico: New Mexico Bureau of Mines and Mineral Resources Geologic Map 48, scale 1:125,000, 1 sheet.

Kellogg, K.S., 1999, Neogene basins of the northern Rio Grande rift: Partitioning and asymmetry inherited from Laramide and older uplifts: Tectonophysics, v. 305, p. 141–152.

Kelson, K.I., and Bauer, P.W., 1998, Geologic map of the Carson quadrangle, Taos County, New Mexico: New Mexico Bureau of Mines and Mineral Resources Open-File Geologic Map 22, 1:24,000 scale, 1 sheet, 6 p. text.

___2003, Geologic map of the Los Cordovas quadrangle, Taos County, New Mexico: New Mexico Bureau of Geology and Mineral Resources Open-File Geologic Map 63, 1:24,000 scale, 1 sheet.

Kelson, K.I., Bauer, P.W., Diehl, K.S., and two others, 2001, Geologic map of the Taos quadrangle, Taos County, New Mexico: New Mexico Bureau of Geology and Mineral Resources Open-File Geologic Map 43, scale 1:24,000, 1 sheet, 9 p. text.

Kelson, K.I., Bauer, P.W., Unruh, J.R., and Bott, J.D.J., 2004, Late Quaternary characteristics of the northern Embudo fault, Taos County, New Mexico, *in* Brister, B.S., Bauer, P.W., Read, A.S., and Lueth, V.W., eds., Geology of the Taos Region: New Mexico Geological Society, 55th Fall Field Conference, Guidebook, p. 147–157.

Kelson, K.I., Unruh, J.R., and Bott, J.D.J., 1997, Field characterization, kinematic analysis, and initial paleoseismic assessment of the Embudo fault, northern New Mexico: Final technical report to U.S. Geological Survey from William Lettis and Associates Inc., 48 p.

Kluth, C.F., 2007, Inversion and reinversion of the northern Rio Grande rift, San Luis Basin, southern Colorado: Geological Society of America Abstracts with Programs, v. 39, no. 6, p. 366.

Kluth, C.F., and Schaftenaar, C.H., 1994, Depth and geometry of the northern Rio Grande rift in the San Luis Basin, south-central Colorado, *in* Keller, G.R., and Cather, S.M., eds., Basins of the Rio Grande rift: Structure, stratigraphy, and tectonic setting: Boulder, Colorado, Geological Society of America Special Paper 291, p. 27–37.

Koning, D.J., and Mansell, M.M., 2011, Regional geologic map of north-central New Mexico, *in* Koning, D.J., Karlstrom, K.E., Kelley, S.A., and two others, eds., Geology of the Tusas Mountains and Ojo Caliente: New Mexico Geological Society, 62nd Fall Field Conference, Guidebook, p. 150–151.

Koning, D.J., Aby, S.B., Grauch, V.J.S., and Zimmerer, M.J., 2016, Latest Miocene–earliest Pliocene evolution of the ancestral Rio Grande at the Española-San Luis Basin boundary, northern New Mexico: New Mexico Geology, v. 38, p. 24–49.

Koning, D.J., Aby, S., and Kelson, K.I., 2007, Geologic map of the Taos Junction quadrangle, Taos County, New Mexico: New Mexico Bureau of Geology and Mineral Resources Open-File Geologic Map 144, scale 1:24,000, 1 sheet, 28 p. text.

Koning, D.J., Ferguson, J.F., Jackson-Paul, P.B., and Baldridge, W.S., 2004, Geologic structure of the Velarde graben and the southern Embudo fault system, north-central N.M., *in* Brister, B.S., Bauer, P.W., Read, A.S., and Lueth, V.W., eds., Geology of the Taos Region: New Mexico Geological Society, 55th Fall Field Conference, Guidebook, p. 158–171.

Kucks, R.P., Hill, P.L., and Heywood, C.E., 2001, New Mexico aeromagnetic and gravity maps and data: A website for distribution of data: U.S. Geological Survey Open-File Report 01-61, https://pubs.usgs.gov/of/2001/ofr-01-0061/.

Kues, B.S., and Giles, K.A., 2004, The Late Paleozoic Ancestral Rocky Mountains System in New Mexico, *in* Mack, G.H., and Giles, K.A., eds., The geology of New Mexico: A geologic history: New Mexico Geological Society, Special Publication 11, p. 95–136.

Downloaded from https://pubs.geoscienceworld.org/uwyo/rmg/article-pdf/54/2/97/4907139/05402097.pdf
by USGS Library, Benjamin Drenth

Large, E., and Ingersoll, R.V., 1997, Miocene and Pliocene sandstone petrofacies of the northern Albuquerque Basin, New Mexico, and implications for evolution of the Rio Grande rift: Journal of Sedimentary Research, v. 67, p. 462–468.

Lipman, P.W., 1975a, Evolution of the Platoro caldera complex and related volcanic rocks, southeastern San Juan Mountains, Colorado: U.S. Geological Survey Professional Paper 852, *v* + 128 p.

___1975b, Geologic map of the lower Conejos River canyon area, southeastern San Juan Mountains, Colorado: U.S. Geological Survey Miscellaneous Investigations Map I-901, scale 1:48,000, 1 sheet.

___1988, Evolution of silicic magma in the upper crust: The mid-Tertiary Latir volcanic field and its cogenetic granitic batholith, northern New Mexico, U.S.A.: Transactions of the Royal Society of Edinburgh, Earth Sciences, v. 79, p. 265–288.

___2007, Incremental assembly and prolonged consolidation of Cordilleran magma chambers: Evidence from the Southern Rocky Mountain volcanic field: Geosphere, v. 3, p. 42–70.

Lipman, P.W., and Mehnert, H.H., 1975, Late Cenozoic basaltic volcanism and development of the Rio Grande depression in the Southern Rocky Mountains, *in* Curtis, B.F., ed., Cenozoic history of the Southern Rocky Mountains: Geological Society of America Memoir 144, p. 119–154.

___1979, The Taos Plateau volcanic field, northern Rio Grande rift, New Mexico, *in* Riecker, R.E., ed., Rio Grande rift: Tectonics and magmatism: Washington, D.C., American Geophysical Union, p. 289–311.

Lipman, P.W., and Reed, J.C., Jr., 1989, Geologic map of the Latir volcanic field, and adjacent areas, northern New Mexico: U.S. Geological Survey Miscellaneous Investigations Series Map I-1907, scale 1:48,000, 2 sheets.

Lipman, P.W., Mehnert, H.H., and Naeser, C.W., 1986, Evolution of the Latir volcanic field, northern New Mexico, and its relation to the Rio Grande rift, as indicated by potassium-argon and fission track dating: Journal of Geophysical Research, v. 91, no. B6, p. 6,329–6,345.

Logsdon, M.J., 1981, A preliminary basin analysis of the El Rito Formation (Eocene), north-central New Mexico: Geological Society of America Bulletin, v. 92, p. 968–975.

Long, C.L., 1985, Regional audiomagnetotelluric study of the Questa caldera, New Mexico: Journal of Geophysical Research, v. 90, p. 11,270–11,274.

Machette, M.N., Personius, S.F., Kelson, K.I., and two others, 1998, Map and data for Quaternary faults and folds in New Mexico: U.S. Geological Survey Open-File Report 98-521, scale 1:750,000, 1 sheet, 358 p. text.

Maldonado, F., 2008, Geologic map of the Abiquiu quadrangle, Rio Arriba County, New Mexico: U.S. Geological Survey Scientific Investigations Map 2998, scale 1:24,000, 1 sheet, 19 p. text.

Manley, K., 1981, Redefinition and description of the Los Pinos Formation of north-central New Mexico: Geological Society of America Bulletin, part one, v. 92, p. 984–989.

___1982a, Geologic map of the Bighorn Peak quadrangle, Rio Arriba County, New Mexico and Conejos County, Colorado: U.S. Geological Survey Miscellaneous Field Studies Map MF-1451, scale 1:24,000, 1 sheet.

___1982b, Geologic map of the Broke Off Mountain quadrangle, Rio Arriba County, New Mexico: U.S. Geological Survey Miscellaneous Field Studies Map MF-1450, scale 1:24,000, 1 sheet.

Manley, K., and Wobus, R.A., 1982a, Reconnaissance geologic map of the Las Tablas quadrangle, Rio Arriba County, New Mexico: U.S. Geological Survey Miscellaneous Field Studies Map MF-1408, scale 1:24,000, 1 sheet.

___1982b, Reconnaissance geologic map of the Mule Canyon quadrangle, Rio Arriba County, New Mexico: U.S. Geological Survey Miscellaneous Field Studies Map MF-1407, scale 1:24,000, 1 sheet.

___1985, Reconnaissance geologic map of the Toltec Mesa quadrangle, Rio Arriba County, New Mexico: U.S. Geological Survey Miscellaneous Field Studies Map MF-1624, scale 1:24,000, 1 sheet.

Manley, K., Scott, G.R., and Wobus, R.A., 1987, Geologic map of the Aztec 1 degree by 2 degrees quadrangle, northwestern New Mexico and southern Colorado: U.S. Geological Survey Miscellaneous Investigations Series Map I-1730, scale 1:250,000, 1 sheet.

Menges, C.M., 1990, Late Cenozoic rift tectonics and mountain-front landforms of the Sangre de Cristo Mountains near Taos, New Mexico, *in* Bauer, P.W., Lucas, S.G., Mawer, C.K., and McIntosh, W.C., eds., Tectonic development of the southern Sangre de Cristo Mountains, New Mexico: New Mexico Geological Society, 41st Fall Field Conference, Guidebook, p. 113–122.

Miller, J.P., Montgomery, A., and Sutherland, P.K., 1963, Geology of part of the southern Sangre de Cristo Mountains, New Mexico: Stratigraphy, structure, and petrology of the Tesuque-Velarde-Tres Ritos-Cowles thirty-minute quadrangle: New Mexico Bureau of Mines and Mineral Resources Memoir 11, *viii* + 106 p., 1 sheet.

Muehlberger, W.R., 1979, The Embudo fault between Pilar and Arroyo Hondo, New Mexico—An active intracontinental transform fault, *in* Ingersoll, R.V., Woodward, L.A., and James, H.L., eds., Santa Fe Country: New Mexico Geological Society, 30th Fall Field Conference, Guidebook, p. 77–82.

Nelson, P.H., and Anderson, L.A., 1992, Physical properties of ash flow tuff from Yucca Mountain, Nevada: Journal of Geophysical Research, v. 97, no. B5, p. 6,823–6,841.

Downloaded from https://pubs.geoscienceworld.org/uwyo/rmg/article-pdf/54/2/97/4907139/05402097.pdf
by USGS Library, Benjamin Drenth

Palacky, G.J., 1987, Resistivity characteristics of geologic targets, *in* Nabighian, M.N., ed., Electromagnetic methods in applied geophysics, v. 1, Theory: Tulsa, Oklahoma, Society of Exploration Geophysicists, p. 53–129.

Pan-American Center for Earth and Environmental Studies, 2006, Online gravity and magnetic database: El Paso, Texas, University of Texas at El Paso: *at* https://research.utep.edu/Default.aspx?alias=research.utep.edu/paces (accessed November 2006).

Personius, S.F., and Machette, M.N., 1984, Quaternary and Pliocene faulting in the Taos Plateau region, northern New Mexico, *in* Baldridge, W.S., Dickerson, P.W., Riecker, R.E., and Zidek, J., eds., Rio Grande rift: Northern New Mexico: New Mexico Geological Society, 35th Fall Field Conference, Guidebook, p. 83–90.

Quaternary Fault and Fold Database of the United States, 2017, Earthquake Hazards Program: Faults, U.S. Geological Survey: *a*t https://earthquake.usgs.gov/hazards/qfaults/ (accessed January 2017).

Read, A.S., Bauer, P.W., Thompson, R.A., and two others, 2004, The Taos plateau and the Rio Grande Gorge—First-day road log from Taos to Questa, the Wild Rivers Recreation Area, Arroyo Hondo, the Dunn Bridge, the Rio Grande Gorge bridge, and return to Taos, *in* Brister, B.S., Bauer, P.W., Read, A.S., and Lueth, V.W., eds., Geology of the Taos Region: New Mexico Geological Society, 55th Fall Field Conference, Guidebook, p. 1–36.

Rehder, T.R., 1986, Stratigraphy, sedimentology, and petrography of the Picuris Formation in Ranchos de Taos and Tres Ritos quadrangles, north-central New Mexico [Master's thesis]: University Park, Texas, Southern Methodist University, 110 p.

Reynolds, R.L., Rosenbaum, J.G., Hudson, M.R., and Fishman, N.S., 1990, Rock magnetism, the distribution of magnetic minerals in the Earth's crust, and aeromagnetic anomalies, *in* Hanna, W.F., ed., Geologic applications of modern aeromagnetic surveys, U.S. Geological Survey Bulletin 1924, p. 24–45.

Robson, S.G., and Banta, E.R., 1995, Ground water atlas of the United States: Segment 2, Arizona, Colorado, New Mexico, Utah: U.S. Geological Survey Hydrologic Investigations Atlas 730-C, 32 p.

Rodriguez, B.D., and Sawyer, D.A., 2013, Geophysical constraints on Rio Grande rift structure and stratigraphy from magnetotelluric models and borehole resistivity logs, northern New Mexico, *in* Hudson, M.R., and Grauch, V.J.S., eds., New Perspectives on Rio Grande Rift Basins: From Tectonics to Groundwater: Boulder, Colorado, Geological Society of America Special Paper 494, p. 323–344.

Ruleman, C., and Machette, M.N., 2007, An overview of the Sangre de Cristo fault system and new insights to interactions between Quaternary faults in the northern Rio Grande rift, *in* Machette, M.N., Coates, M.M., and Johnson, M.L., eds., 2007 Rocky Mountain Section Friends of the Pleistocene field trip—Quaternary geology of the San Luis Basin of Colorado and New Mexico, September 7–9, 2007: U.S. Geological Survey Open-File Report 2007-1193, p. 187–197.

Ruleman, C.A., Thompson, R.A., Shroba, R.R., and four others, 2013, Late Miocene–Pleistocene evolution of a Rio Grande rift subbasin, Sunshine Valley-Costilla Plain, San Luis Basin, New Mexico and Colorado, *in* Hudson, M.R., and Grauch, V.J.S., eds., New Perspectives on Rio Grande Rift Basins: From Tectonics to Groundwater: Boulder, Colorado, Geological Society of America Special Paper 494, p. 47–73.

Sales, J.K., 1983, Collapse of Rocky Mountain basement uplifts, *in* Lowell, J.D., ed., Rocky Mountain foreland basins and uplifts: Denver, Colorado, Rocky Mountain Association of Geologists, p. 79–97.

Simpson, R.W., Jachens, R.C., Blakely, R.J., and Saltus, R.W., 1986, A new isostatic residual gravity map of the conterminous United States with a discussion on the significance of isostatic residual anomalies: Journal of Geophysical Research, v. 91, no. B8, p. 8,348–8,372.

Smith, G.A., 2004, Middle to late Cenozoic development of the Rio Grande rift and adjacent regions in northern New Mexico, *in* Mack, G.H., and Giles, K.A., eds., The Geology of New Mexico, A geologic history: New Mexico Geological Society, Special Publication 11, p. 331–358.

Smith, G.A., Moore, J.D., and McIntosh, W.C., 2002, Assessing roles of volcanism and basin subsidence in causing Oligocene–lower Miocene sedimentation in the northern Rio Grande rift, New Mexico, USA: Journal of Sedimentary Research, v. 72, p. 836–848.

Spiegel, Z., and Baldwin, B., 1963, Geology and water resources of the Santa Fe area, New Mexico: U.S. Geological Survey Water-Supply Paper 1525, *xiii* + 258 p.

Steven, T.A., 1975, Middle Tertiary volcanic field in the Southern Rocky Mountains, *in* Curtis, B.F., ed., Cenozoic history of the Southern Rocky Mountains: Geological Society of America Memoir 144, p. 75–94.

Tappa, M.J., Coleman, D.S., Mills, R.D., and Samperton, K.M., 2011, The plutonic record of a silicic ignimbrite from the Latir volcanic field, New Mexico: Geochemistry, Geophysics, Geosystems, v. 12, no. 10, 16 p.

Thompson, R.A., and Lipman, P.W., 1994, Geologic map of the Los Pinos quadrangle, Rio Arriba and Taos counties, New Mexico, and Conejos County, Colorado: U.S. Geological Survey Geologic Quadrangle Map GQ-1749, scale 1:24,000, 1 sheet.

Thompson, R.A., and Machette, M.N., 1989, Geologic map of the San Luis Hills area, Conejos and Costilla counties, Colorado: U.S. Geological Survey Miscellaneous Investigations Series Map I-1906, scale 1:50,000, 1 sheet.

Downloaded from https://pubs.geoscienceworld.org/uwyo/rmg/article-pdf/54/2/97/4907139/05402097.pdf
by USGS Library, Benjamin Drenth

Thompson, R.A., and Schilling, S.P., 1988, Generalized geologic maps of the Brushy Mountain and Timber Mountain areas, Taos County, New Mexico: U.S. Geological Survey Open-File Report 88-561, undefined scale, 1 sheet.

Thompson, R.A., Dungan, M.A., and Lipman, P.W., 1986, Multiple differentiation processes in early-rift calc-alkaline volcanics, northern Rio Grande rift, New Mexico: Journal of Geophysical Research, v. 91, no. B6, p. 6,046–6,058.

Thompson, R.A., Johnson, C.M., and Mehnert, H.H., 1991, Oligocene basaltic volcanism of the northern Rio Grande rift: San Luis Hills, Colorado: Journal of Geophysical Research, v. 96, no. B8, p. 13,577–13,592.

Thompson, R.A., Shroba, R.R., Machette, M.N., and three others, 2015, Geologic map of the Alamosa 30′ × 60′ quadrangle, south-central Colorado: U.S. Geological Survey Scientific Investigations Map 3342, scale 1:100,000, 1 sheet, 23 p. text, http://dx.doi.org/10.3133/sim3342.

Thompson, R.A., Turner, K.J., Cosca, M.A., and four others, in press, IAVCEI RGR-SRMVF Day 2: Southern San Luis Basin and Taos Plateau volcanic field: Field-trip guides to selected volcanoes and volcanic landscapes of the western United States: U.S. Geological Survey Scientific Investigations Report 2017-5022-R, p. 42–103.

Topper, R., Spray, K.L., Bellis, W.H., and two others, 2003, Ground water atlas of Colorado: Colorado Geological Survey, Special Publication 53, 210 p.

Turner, K.J., Thompson, R.A., Chan, C.F., and three others, in press, IAVCEI RGR-SRMVF Day 3: Taos Plateau volcanic field and central San Luis Basin: Field-trip guides to selected volcanoes and volcanic landscapes of the western United States: U.S. Geological Survey Scientific Investigations Report 2017-5022-R, p. 104–149.

Turner, K.J., Thompson, R.A., Cosca, M.A., and three others, 2018, Geologic map of the San Antonio Mountain area, northern New Mexico and southern Colorado: U.S. Geological Survey Scientific Investigations Map 3417, scale 1:50,000, 1 sheet, https://pubs.er.usgs.gov/publication/sim3417.

Vening-Meinesz, F.A., 1950, Les 'grabens' africains, resultat de compression ou de tension dans la croute terrestre? [The African 'grabens', result of compression or tension in the Earth's crust]: Bulletin of the Royal Colonial Institute of Belgium, v. 21, p. 539–552.

Vozoff, K., 1991, The magnetotelluric method, *in* Nabighian, M.N., ed., Electromagnetic methods in applied geophysics, v. 2, Application, part B: Tulsa, Oklahoma, Society of Exploration Geophysicists, p. 641–711.

Wernicke, B., and Axen, G.J., 1988, On the role of isostasy in the evolution of normal fault systems: Geology, v. 16, 848–851.

Williams, M.L., 1991, Heterogeneous deformation in a ductile fold-thrust belt: The Proterozoic structural history of the Tusas Mountains, New Mexico: Geological Society of America Bulletin, v. 103, p. 171–188.

Winograd, I.J., 1959, Ground-water conditions and geology of Sunshine Valley and western Taos County, New Mexico: U.S. Geological Survey Technical Report 12, 70 p., 2 sheets.

Wobus, R.A., and Manley, K., 1982, Reconnaissance geologic map of the Burned Mountain quadrangle, Rio Arriba County, New Mexico: U.S. Geological Survey Miscellaneous Field Studies Map MF-1409, scale 1:24,000, 1 sheet.

Woodward, L.A., Anderson, O.J., and Lucas, S.G., 1999, Late Paleozoic right-slip faults in the Ancestral Rocky Mountains, *in* Pazzaglia, F.J., and Lucas, S.G., eds., Albuquerque Geology: New Mexico Geological Society, 50th Fall Field Conference, Guidebook, p. 149–153.

Zimmerer, M.J., and McIntosh, W.C., 2012, The geochronology of volcanic and plutonic rocks at the Questa caldera: Constraints on the origin of caldera-related silicic magmas: Geological Society of America Bulletin, v. 124, p. 1,394–1,408.

Scientific Editors: Arthur W. Snoke and B. Ronald Frost

Downloaded from https://pubs.geoscienceworld.org/uwyo/rmg/article-pdf/54/2/97/4907139/05402097.pdf
by USGS Library, Benjamin Drenth

Downloaded from https://pubs.geoscienceworld.org/uwyo/rmg/article-pdf/54/2/97/4907139/05402097.pdf
by USGS Library, Benjamin Drenth